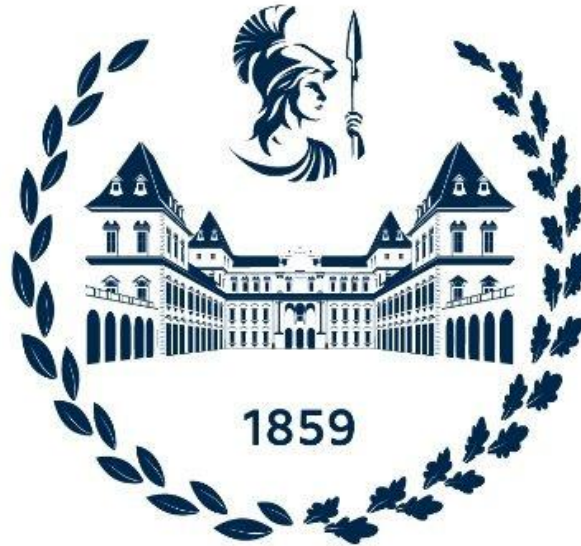


POLITECNICO DI TORINO

Corso di Laurea Magistrale in Ingegneria Meccanica (Mechanical Engineering)



Master's Degree Thesis

Monitoring and Life Assessment of the Gearbox

Supervisors:

Prof. Eugenio Brusa

Prof. Carlo Rosso

Candidate:

Anshu Yadav Kumar

October 2021

Contents

Abstract.....	4
Introduction	5
1.Literature	7
1.1 Some types of gear damages and methodologies to find them.....	7
1.1.1 Tooth Crack damage: Hilbert Empirical Wavelet Transform	7
1.1.2 Gear surface pitting damages: Integrating Oil Debris and Vibration technologies	8
1.1.3 Detecting Gear tooth fatigue cracks in advance of complete fracture: By method FM48	
1.1.4 Bearing defect Identification: By using Acoustic Emission Techniques	9
1.2 Wear failure and its types in gears	10
1.2.1 Adhesive wear.....	11
1.2.2 Abrasive wear.....	11
1.2.3 Corrosive wear	12
1.2.4 Fatigue wear.....	13
1.3 Pitting and its types in gears	13
1.3.1 Initial pitting.....	14
1.3.2 Destructive or progressive pitting.....	15
1.3.3 Normal dedendum pitting	16
2.Correlation between oil debris amount and failure mechanism.....	17
2.1 First part: Correlation between debris amount and wear:.....	17
2.1.1 Example to test the model of wear:	19
2.1.2 Sensitivity analysis of the model:.....	20
2.2 Correlation between oil debris amount and pitting:	23
2.2.1 PCr Criterion.....	23
2.2.2 Findley Criterion:.....	26
Critical Plane approach:	27
3.Results Validation:	47
3.2 Case 1- By using non-realistic values of contact pressures:	47
3.3 Case 2- By using realistic values of contact pressures:	53
Conclusion	59
Bibliography	60

Acknowledgement:

First of all, I would like to thank Prof. Eugenio Brusa and Prof. Carlo Rosso for the patient guidance, encouragement and advice they have provided throughout my thesis work.

Last but not least, I would like to thank all of my family members and friends and the people I love for their unconditional support, timely motivation.

Abstract

This MSc. thesis has been carried out at the university Politecnico di Torino.

As, early failure detection has been an integral part of condition monitoring of critical systems, such as wind turbines, helicopter rotor drivetrains etc. On many occasions, driveline components fail catastrophically, leaving no evidence of the root cause of failure and causing extensive damage to test equipment. This can be avoided by detecting failure in early stages. Most of failure detection techniques are based on oil debris monitoring of gears.

The objective of this thesis is to find a correlation between oil debris amount and failure mechanism. This task has been divided into two parts.

The aim of the first part is to find correlation between debris amount and wear, whereas the aim of the second part is to find correlation between debris amount and pitting, so the mathematical model that has to be developed is the correlation between number of cycles to failure (so the starting events for the production of debris) and the contact stress.

As each engagement reduces the life of the teeth, when the damage factor is equal to one, the possibility to have debris is reached. If debris comes earlier than this number of cycles, the debris is surely caused by the wear, if not, it is related principally to the rolling contact fatigue, so pitting. The aim of mathematical model is to compute the number of cycles to failure for pitting and this has been implemented by using MATLAB code, where the task is to find the maximum damage factor that a contact path along the mesh cycle generates in a tooth.

Introduction

Monitoring the condition of gearboxes is essential to guarantee the machine integrity for their whole designed lifetime. Gearbox is one of the most important components in mechanical equipment during industrial processes. Its health and safety are vital to reliable operation and improved efficiency of relevant facilities in the whole system. The failure rate of transmission gearbox in wind farms ranges from 40% to 50%. In the aerospace industry, approximately 68% of helicopter accidents are attributed to the transmission system, which accounts for 58% of the total maintenance cost.[2]

However, gearboxes generally work under harsh operating environment, which may accelerate their degradation. Consequently, they are subjected to different defect types such as gear fatigue crack, gear pitting, bearing defects, bent shaft etc. Gearbox defects may cause failure of the whole system leading to significant economic losses, costly downtime, and even catastrophic damage. Thus, fault diagnosis and prognosis of gearboxes are of great importance to achieve a high degree of availability, operational safety, and reliability.

In gearbox condition monitoring, a variety of sensing techniques have been instrumented to acquire gearbox mechanical components conditions. These sensing techniques are categorized into direct and indirect sensing methods:

1. Direct sensing techniques measures actual quantities that directly indicate gearbox mechanical components conditions. For example, Oil debris mass, Inductance type oil debris sensors count particles and approximate debris size and mass based on disturbances of a magnetic field caused by passage of a metallic particle.
2. Indirect sensing techniques measure the auxiliary in-process quantities, for example vibration, acoustic emission, etc. that indirectly indicate gearbox components conditions. At present vibration sensors have been the most commonly used sensors in mechanical systems health monitoring application.

Gears are essential machine elements designed to transmit motion and power from one mechanical unit to another. There hardly exists any engineering machine that operates without gears. Various types of gear have been developed to perform different functions. The major types are spur gears, helical gears, straight and spiral

bevel gears, and hypoid gears. The gear type and the specific design features determine the operating characteristics of a gear.[1]

Approximately, 60% of the gear damages are caused by the fatigue damage of teeth. Variable, cyclic, loading of the gear teeth can cause the initiation of fatigue cracks at the tooth base and later a crack at the tooth base. Fatigue cracks may appear in the tooth base in these places, which are subjected to the greatest stress. Their location can be determined on the basis of numerical analysis, taking into account the variability of the meshing force, the point (line) of its application and its direction due to impaired cooperating gear pairs. This thesis will be focused on condition monitoring of one component of gearbox called gears.

1.Literature

Gearboxes or also commonly called gear reducers or enclosed speed reducers are used on many electromechanical drive systems. The gearboxes are essentially multiple open gear sets contained in a housing. The housing supports bearings and shafts, holds in lubricants, and protects the components from surrounding conditions. Gearboxes are available in a wide range of load capacities and speed ratios. The purpose of the gearbox is to increase or reduce the speed.

1.1 Some types of gear damages and methodologies to find them

Here we will discuss briefly some typical gear damages and methodologies to find them:

1.1.1 Tooth Crack damage: Hilbert Empirical Wavelet Transform

Hilbert-Huang transform (HHT) is composed of two main parts: the empirical mode decomposition (EMD), and the Hilbert Transform (HT). The EMD is an intuitive, unsupervised, and self-adaptive method that can decompose a non-stationary and non-linear signal into narrow-band oscillatory components called Intrinsic Mode Functions (IMFs). An IMF is defined as a function having the same local extrema and zero-crossing number or differ by 1 at most, and also having symmetric envelopes defined by the local maxima, and minima respectively.

However, in practical applications, the HHT has some unsolved problems which are caused by the EMD technique. The EMD has the problem of mixing which means waves with the same frequency are assigned to different IMFs, and it causes the End Effect phenomenon, which leads to wrong instantaneous values at both sides of the signal. On the other hand, it adds a false Intrinsic Mode Functions IMFs causelessly, moreover its lack of mathematical basis.

Gilles (2013) developed a new method called Empirical Wavelet Transform (EWT) which designs an appropriate wavelet filter bank to extract amplitude and frequency modulation components of a signal. He demonstrated that the EWT is better than the EMD technique.

To overcome HHT difficulties a new method was proposed for gearbox condition monitoring, which is a merger of the EWT and HT. The application concerns, particularly the early gear tooth crack fault detection in both noisy and non-noisy environments. The EWT is used to extract adaptive modes from the vibration signals and then the instantaneous frequencies are performed of each mode using HT. This combination is denoted as Hilbert Empirical Wavelet Transform (HEWT).

1.1.2 Gear surface pitting damages: Integrating Oil Debris and Vibration technologies

Vibration analysis: All machines with moving parts give rise to sound and vibration. Each machine has a specific vibration signature related to the construction and the state of the machine. If the state of the machine changes, the vibration signature will also change. A change in the vibration signature can be used to detect incipient defects before they become critical. Examples of widely used techniques for gearbox are such as Waveform analysis, Time-Frequency analysis, Faster Fourier Transform (FFT)analysis, Spectral analysis, Order analysis, Time Synchronous Average, and probability density moments analysis.

Oil-Debris Monitoring (ODM): A commercially available in-line oil debris monitor is used to measure metallic content generated in the lubrication system due to the mechanical component fatigue failures. The ODM sensor element consisted of three coils that surrounded a non-conductive section of tubing. The two outside field coils were oppositely wound and driven by an AC current source. The centre coil measured the disturbance to the magnetic fields caused by the passage of metallic particles through the sensor. The disturbance was proportional to the size of the particles.

A diagnostic tool for detecting damages to gears was developed. Two different measurement technologies, debris analysis and vibration, were integrated into a health monitoring system for detecting surface pitting damage on gears. This integrated system showed improved detection and decision-making capabilities as compared to using individual measurement technologies. This diagnostic tool was developed and evaluated experimentally by collecting vibration and oil debris data from fatigue tests performed in the NASA Glenn Spur Gear Fatigue Test Rig. Vibration data can be collected from accelerometers and oil debris data can be collected using a commercially available in-line oil debris sensor.

1.1.3 Detecting Gear tooth fatigue cracks in advance of complete fracture: By method FM4

This method was developed to detect changes in the vibration pattern resulting from damage on a limited number of teeth. A difference signal is first constructed by removing the regular meshing components (shafts frequency and harmonics, primary meshing frequency, and harmonics along with their first order sidebands) from the time-averaged signal. The fourth normalized statistical moment (normalized kurtosis) is then applied to this difference signal. For a gear in good

condition the 2-difference signal would be primarily Gaussian noise, resulting in a normalized kurtosis value of 3. When one or two teeth develop a defect (such as crack, or pitting), a peak or series of peaks appear in the difference signal, causing the normalized kurtosis value to increase beyond the nominal value of 3.

1.1.4 Bearing defect Identification: By using Acoustic Emission Techniques

Acoustic Emission Techniques: The gearbox is one of the most critical parts of a helicopter. During the flight, the main gearbox suffers from high temperature and stress as a substantial amount of frictional heat is generated when the input high rotation speed of gas turbines is converted to low speed, high torque within the gearbox. The malfunction of the gearbox can cause serious disaster due to the lack of redundancy of transmission system in a helicopter. The operating condition of gearbox is usually monitored by using vibration and temperature sensors in helicopter health and usage monitoring systems (HUMS). These sensors are usually mounted on casing to avoid complex wiring. However, vibration signal might be significantly attenuated if target bearing, or gear is far from gearbox housing. The indirect measurement could not provide an accurate temperature. So, in addition to external vibration analysis, internal Acoustics Emissions (AE) technology is also employed to identify a fault condition. AE provides the benefit of early fault detection in comparison to vibration analysis and oil analysis because of the high sensitivity to friction offered by AE. AE sensors detect stress wave that propagates through the material when crack surfaces are formed. As the crack propagates, the frequency of the stress wave increases, and these activities are monitored by the AE sensor. AE is suitable for detecting the early stages of crack initiation. Ideally, an AE sensor has to be close to its source to avoid severe attenuation and reflections. However, it is often only practical to place an AE sensor on the non-rotating parts of the machine, such as the bearing housing or gearbox casing. In order, to solve the issues of indirect measurement and complex wiring inside gearbox, an AE sensor has to directly attach on the target bearing and the acquired signal can be transmitted wirelessly.

1.2 Wear failure and its types in gears

Gear wear refers to the progressive material loss from contacting tooth surfaces due to the combined rolling and the sliding motion under mixed or boundary lubrication conditions. It is one of the major failure modes of gears. The direct results of gear wear include dynamic transmission error, power transmission losses, and high vibration and noise levels. Severe wear can also cause uneven load distributions, which could lead to the occurrence of other types of gear failure, such as broken teeth. For these reasons, the topic of gear wear monitoring is receiving considerable attention in the condition monitoring community. If critical wear occurs on the tooth surface, the following phenomena occurs:

1. Increase of noise or vibration.
2. Excessive increase in temperature at the gear device.
3. Increase of smear by the lubricant.
4. Increase of backlash.

By properly removing the cause of these troubles, damage can be avoided.

The following introduces causes of tooth damage and solutions to overcome the problem:

a. When the tooth surface strength is insufficient against the load.

Solution: 1. Increasing the strength of the tooth surface, by enlarging the gear size, or by enlarging the face-width, or change the material to stronger material having more hardness.

Solution: 2. Decreasing the load by changing the driving conditions.

b. Improper tooth contact caused by bad mounting.

Solution: Adjusting the tooth contact.

c. When partial contact occurs due to bad mounting.

Solution: Change design of the gear, shaft and bearing to make them stronger. By increasing stiffness, tooth contact improves.

d. When lubrication is in a poor condition

Solution: Provide appropriate conditions for the lubricant; proper type, viscosity, and quantity.

1.2.1 Adhesive wear

It is also known as scuffing or galling, and may occur under boundary lubrication conditions, when two surfaces get “bonded” during a sliding movement (metal-to-metal contact). When the two surfaces separate, the bonded spot breaks off and removes material from the surfaces, causing fractures, cavities, and tiny abrasive particles which are released. Excessive load, low velocity movements or reduced oil/film viscosity are the typical causes of adhesion.

The influencing factors are: oil film thickness and viscosity; high loads, slow speed; gear tooth size; surface roughness; improper use of anti-scuff and AW/EP additives.

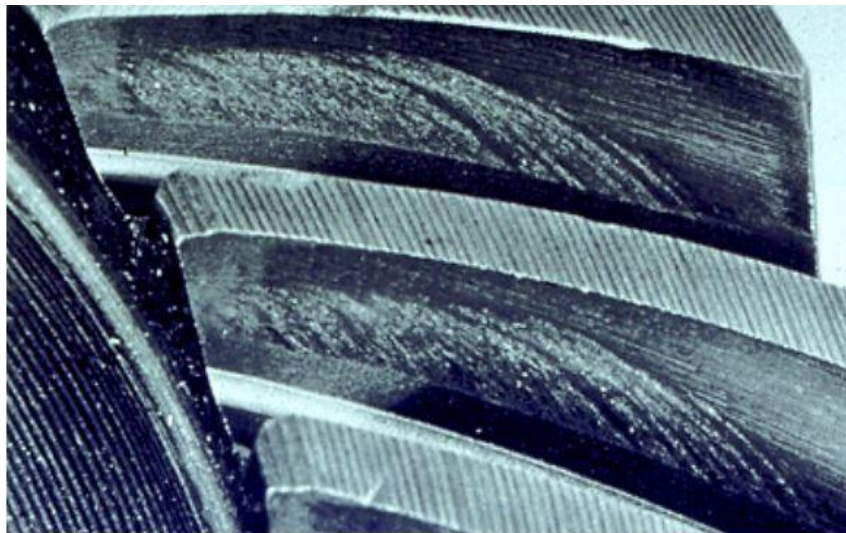


Figure 1: adhesive wear on gear teeth ^[3]

1.2.2 Abrasive wear

It occurs in sliding contact and is also known as grinding, because the wear mechanism is basically the same as the machining, grinding, polishing or lapping used for the shaping of materials.

Two- body abrasive wear occurs when one surface cuts away from the other surface, although this mechanism very often changes to three-body abrasion as the wear debris in turn act as abrasive particles between the two surfaces.

The influencing factors are: oil film thickness, surface hardness, component alignment.

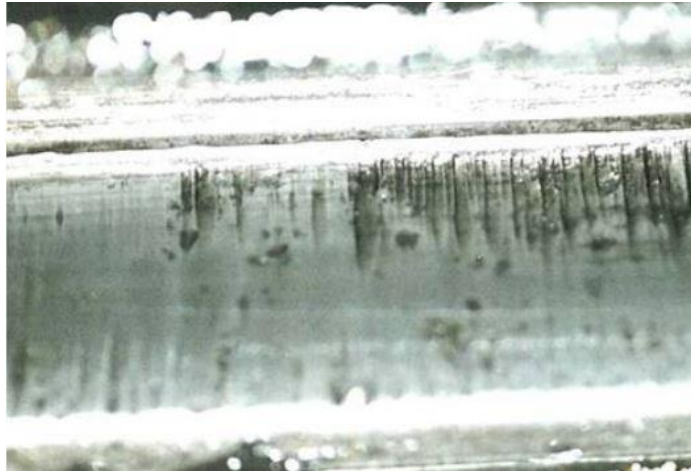


Figure 2 abrasive wear on gear tooth [3]

1.2.3 Corrosive wear

It occurs when there is a combination of a wear situation (abrasive or adhesive) and a corrosive environment. Most lubricants get acidic over time due to the degradation or oxidation processes. Water or moisture reacts with the acid in oil to increase the corrosive potential and further stimulate the attack on metal surfaces. The corrosive wear results in a removal of metal, mostly in the form of ferrous oxides, also known as rust particles. The rate of material loss can be very high, many times more than what would result from the individual processes of wear or corrosion alone.



Figure 3 corrosive wear [3]

1.2.4 Fatigue wear

On components in oil systems, it is usually initiated by cracks and notches, which are the result of particles being trapped and squeezed in the clearance between two surfaces (abrasive wear). Operation of the component being lubricated with oil cause metal stress and may lead to cracks spreading under the surface, due to repeating load and pressure. The result is metal fatigue that the surface will eventually fail and the structure collapse, releasing lots of particles into the oil.

Fatigue wear is mostly seen in oil systems with the rolling element/ball bearings, cams, rollers, and gears exposed to cyclic stress variations, for example at the pitch line of heavy loaded wind turbine gear.



Figure 4 fatigue wear of wind turbine gear^[3]

1.3 Pitting and its types in gears

Pitting is the surface fatigue failure of the gear tooth. It occurs due to repeated loading of tooth surface and the contact stress exceeding the surface fatigue strength of the material. It may occur soon after the operation begins. There are many shrinkage pools on the surface of the gear, especially around the pitch, similar to the condition of eroded. Within the continuity of operation time, the little pools continue to extend; at the same time, the pitting is larger and larger. A lot of falling off blocks distributing in the gearbox, until the gear is totally damaged. It obviously belongs to chronic damage and surface fatigue of gear surface.

Reasons:

1. Because of the improper consideration of texture, hardness, and load, the actually born load exceeds than the surface endurance limit of the gear.
2. The harden layer on the surface is crispy, and it is easier for the occurrence of the hole erosion when the hardness core is too soft.
3. The hardness layer on the surface of the gear is too tiny and thin, and cannot bear the surface pressure, and the crack generates which invokes to surface peeling.

Countermeasures:

1. Take sufficient consideration on the depth of the hardening layer during heat treatment, to ensure sufficiently hardening layer, to keep the gear surface strength.
2. Adopt surface pressure strength, i.e., Hertz surface pressure calculation formula to re-verify the design.
3. Especially, as for the carburized gear surface, in consideration that the core material is low-carbon soft tissue, which cannot bear the surface pressure from the hard surface of the gear surface and leads to surface crazing and hole erosion; therefore, it is necessary to pay special attention to the depth of the carburized layer, and the insufficient carburized layer gives rise to the insufficient surface pressure strength which leads to hole erosion.

1.3.1 Initial pitting

It is caused by local areas of high stress due to uneven surfaces on gear teeth. This type of pitting can develop very short time, reach a maximum. Initial pitting usually occurs in a narrow band at the pitch line or just slightly below the pitch line.

Initial pitting is usually caused by gear tooth surfaces not properly conforming with each other or not fitting together properly. This can be the result of minor involute errors or local surface irregularities, but most often it occurs because there is not proper alignment across the full-face width of the gear mesh.

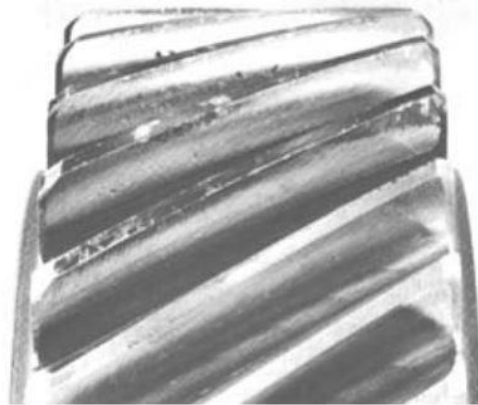


Figure 5 Initial (corrective) pitting^[4]

1.3.2 Destructive or progressive pitting

In this type of pitting the surface pits are usually considerably larger in diameter than those associated with initial pitting. It usually starts below the pitch line, in the dedendum section of the drive gear tooth and progressively increases both in size and number of pits until the surface is destroyed.

Destructive pitting can appear to be as severe as corrective pitting at the beginning of the operation, however as time goes on the severity of destructive pitting sharply increases and far surpasses severity of corrective pitting.

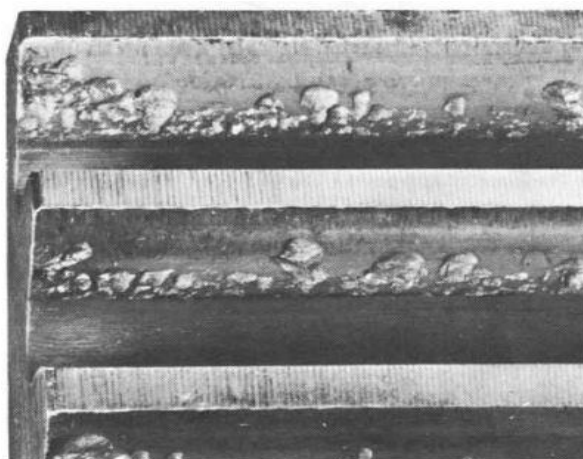


Figure 6 destructive pitting^[4]

1.3.3 Normal dedendum pitting

Dedendum pitting results when loads are at close to maximum allowable surface loading values. The dedendum are most vulnerable to this phenomenon because of the preferential orientation of the surface microcracks along the tooth profile.

At loadings currently used for industrial surface hardened gears, pitting is much less prevalent than with through-hardened gears. When it does occur, the appearance may be similar to that of through-hardened gears, but it often looks different.

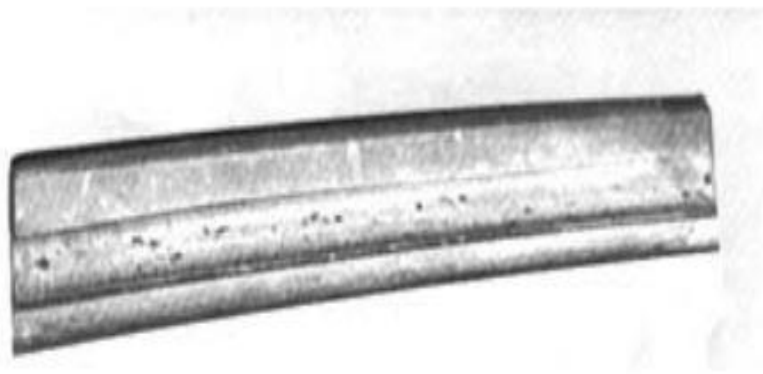


Figure 7 Normal dedendum pitting^[4]

2. Correlation between oil debris amount and failure mechanism

2.1 First part: Correlation between debris amount and wear:

Gear transmissions play an important role in modern technology. They transfer both power and motion with efficiency and appears in various kinds of machinery and control systems. The interaction between gear teeth in a transmission may be affected by wear in negative fashion causing non-uniform gear rate, increasing dynamic effects, decreasing efficiency and possibly severe tooth failure. In order to find the volume of the worn away material, Archard's model has been proposed with some modifications by using combination of other model such as Fleischer model.

While the Fleischer model is based on energetic approaches, the Archard formulation uses an empirical factor-the wear coefficient-describing the intensity of wear. This model has been taken from the article "*Energy-Based Modelling of Adhesive Wear in the Mixed Lubrication Regime*, J. Torben, Mohamed Ali Fourati, Florian Pape and Gerhard Poll".

This model has been supported by the example of meshing between two spur gears, gear and pinion and then performed sensitivity analysis by changing each factor of the model and see how its effecting the volume of worn material.

Neglecting chemical effects, the occurring wear volume can be described by probabilistic models, such as Archard model. Archard as well assumes spherically shaped asperities with a radius of r , such that position i a circular contact area of $A_R^i \approx \pi r^2$ between a pair of contacting asperities forms. He furthermore assumes this area to be so small that the occurring local pressure p^i immediately reaches the yield stress p_{lim} of the surface material. The yield stress can be equated with the surface hardness H , which leads to the relation $H = f^i / A_R^i$. Since each asperity in contact is loaded by the yield stress, this relation holds for all contact spots. The volumes of evolving wear particles can each be represented by the volume of a detached asperity, which equals a hemisphere: $V_W^i = 2/3\pi r^3$. Defining additionally a micro sliding path in the length of the asperity diameter, $S_W^i = 2r$, a local relative wear volume can be defined as:

$$\frac{S_W^i}{V_W^i} = \frac{1}{3} \pi r^2 = \frac{1}{3} A_R^i = \frac{1}{3} \frac{f^i}{H} \quad (2.1)$$

By accumulation of all local relative wear volumes for the entire contact area and considering the force equilibrium for Z asperities, $\sum_{i=1}^Z f^i = F_N$, and the total relative wear volume can be given as:

$$\frac{V_W}{S_W} = \sum_{i=1}^Z \frac{V_W^i}{S_W^i} = \frac{1}{3} \sum_{i=1}^Z \frac{f^i}{H} = \frac{1}{3} K_1 \frac{F_N}{H} \quad (2.2)$$

K_1 takes into account that an instant formation of wear does not occur for every contact. Using the simplification $K = K_1/3$.

The total wear volume can be defined as:

$$V_W = K \frac{F_N S_W}{H} \quad (2.3)$$

where:

- F_N is the total normal force working on the considered system
- S_W is the total sliding path
- K is the Archard Wear Coefficient
- H is the surface hardness

And performed frictional work can be defined as:

$$W_R = \mu F_N S_W \quad (2.4)$$

where:

- μ is the friction coefficient.

The intensity of the wear is described by the apparent frictional energy density e_R^* , and this leads to the Fleischer wear equation:

$$V_W = \frac{W_R}{e_R^*} \quad (2.5)$$

Now we can get the apparent frictional energy density can be given as function of the Archard Wear coefficient and vice versa:

$$e_R^* = \frac{1}{K} \mu H \quad \text{or,} \quad K = \frac{1}{e_R^*} \mu H \quad (2.6)$$

The wear coefficient K can be understood as the probability for the detachment of a single wear particle.

2.1.1 Example to test the model of wear:

Given data: Considering meshing between one gear and pinion.

- Number of teeth of pinion: $Z_1 = 20$
- Power transmitted through pinion = 5kW
- Rotational speed of pinion: $N_1 = 1500$ rpm
- Module = 8mm
- Pressure angle: $\alpha = 20$
- Transmission ratio: $i = \frac{Z_2}{Z_1} = 2.5$

1) Number of teeth required for gear: $Z_2 = i * Z_1 = 2.5 * 20 = 50$ teeth

2) Pitch circle diameters:

$$D_1 = m * Z_1 = 8 * 20 = 160 \text{ mm}$$

$$D_2 = m * Z_2 = 8 * 50 = 400 \text{ mm}$$

3) Addendum = $m = 8$ mm

$$\text{Dedendum} = 1.25 * m = 10 \text{ mm}$$

4) Transmitted Torque:

- As power transmitted: $P = \frac{2 * \pi * N_1 * T_1}{60}$

- And $T_1 = M_{t1} = \frac{5 * 10^3 * 60}{2 * \pi * 1500} = 31.83 \text{ Nm}$

- Similarly, $T_2 = 79.58 \text{ Nm}$

5) Tangential forces:

- $F_{t1} = \frac{2 * M_{t1}}{d_1} = 397.87 \text{ N}$

- $F_{t2} = \frac{2 * M_{t2}}{d_2} = 397.9 \text{ N}$

6) Resultant force or normal force F_N :

- $F_N = \frac{2 * M_{t2}}{d_2 * \cos \alpha} = 423,44 \text{ N}$

7) Length of path of contact which is equivalent to sliding path:

- R : pitch circle radius of gear = 200 mm

- r : pitch circle radius of pinion = 80 mm

- R_A : Gear addendum circle radius = 208 mm

- r_A : Pinion addendum circle radius = 88 mm

- Sliding path: $L = S_w = \sqrt{R_A^2 - R^2 * \cos^2 \alpha} - R * \sin \alpha + \sqrt{r_A^2 - r^2 * \cos^2 \alpha} - r * \sin \alpha = 77 \text{ mm}$,

➤ Sliding path is considered as path of contact between two teeth.

By assuming:

- $\mu = 0.05$
- e_R^* (apparent frictional energy density) = $10^9 \frac{J}{m^3}$,

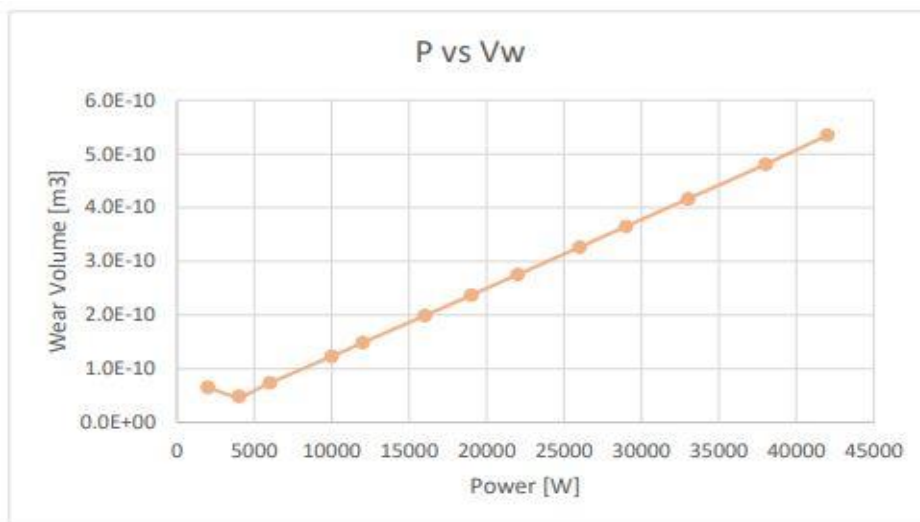
Then,

$V_W = \frac{\mu F_N S_W}{e_R^*} = 1.64 \cdot 10^{-9} m^3$, and this value is near to realistic values of wear particles volume.

2.1.2 Sensitivity analysis of the model:

To investigate how each model's input effect in determining its output.

- **Transmitted power (P):**



- It's an increasing trend because as transmitted power increases normal force increases too, so we will have more loss of material due to wear.

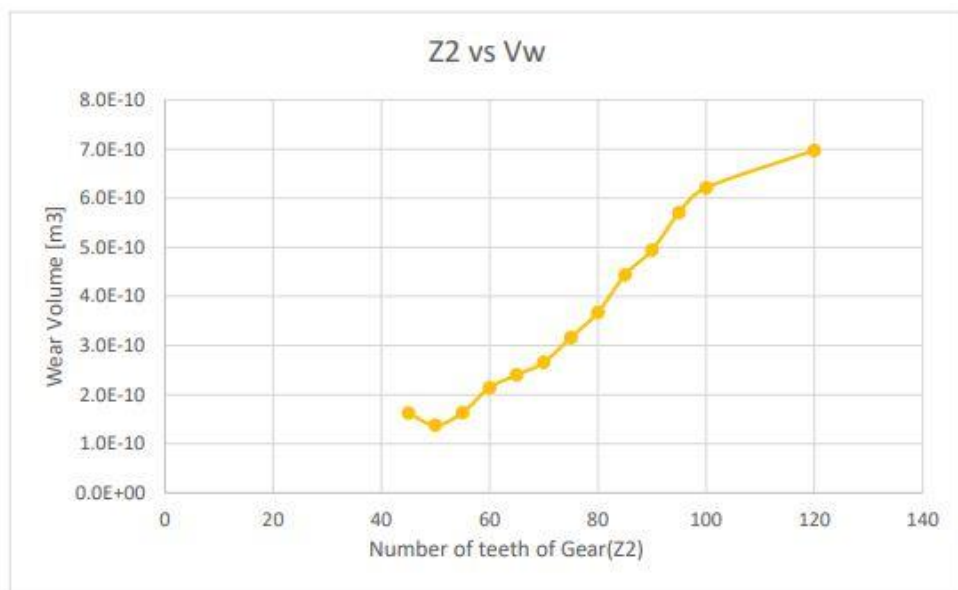
2. Correlation between oil debris amount and failure mechanism

- **Speed of gear**



- It's a decreasing trend because wear volume and speed of gear are inversely proportional according to the relationship, we have found in the previous example of meshing between two spur gear teeth.

- **Number of teeth of gear:**



- It's an increasing trend because if number of teeth of gear increases the tangential speed increases which causes increase in wear volume.

- **Module:**
 - If module increases, the value of contact force decreases, so wear volume decreases too and thus it would be a decreasing trend. The module is very important factor because for gears to mate together they both should have the same module size.

2.2 Correlation between oil debris amount and pitting:

There are two criterions that has been chosen from the article “*A Survey on evaluating the fatigue limit under multiaxial loading, Jan Papuga*” to evaluate the maximum damage factor at contact path along the mesh cycle generates in a tooth in order to compute the number of cycles that the gear can run before having pitting. These two criterions are explained below and the steps to find maximum damage factor from each criterion are:

2.2.1 PCr Criterion

Papuga PCr criterion was introduced in full detail by Papuga and Ruzicka. It uses the hybrid combination of shear stress amplitude quadrate and linear normal stress amplitude. This criterion was the only one that nearly gets to a fatigue index error in range $<-20; 20>\%$. Also, this method has the lowest standard deviation, which is important from an experimental point of view.

$$\sqrt{a_{PC} * C_a^2 + b_{PC}(N_a + d_{PC} * N_m)} \leq f_{-1} \quad (2.7)$$

where:

- C_a is the shear stress on an examined plane (MPa)
- N_a is the amplitude normal stress on an examined plane (MPa)
- N_m is the mean value normal stress on an examined plane (MPa)
- f_{-1} is fatigue limit in fully reversed axial loading (MPa)
- f_0 is fatigue limit in repeated axial loading (MPa)
- t_{-1} is fatigue limit in fully reversed torsion (MPa)
- t_0 is fatigue limit in repeated axial loading (MPa)

Indices:

- a: amplitude
- m: mean value

Coefficients:

- $a = \frac{\kappa^2}{2} + \frac{\sqrt{\kappa^4 - \kappa^2}}{2}$
- $b = f_{-1}$
- $d = \frac{t_{-1}}{f_0}$

and κ is fatigue limit ratio: $\kappa = \frac{f_{-1}}{t_{-1}} [-]$

1) f_{-1} can be considered: $f_{-1} = \frac{R_m}{2}$, where R_m is ultimate tensile strength of the material.

2) t_{-1} can be evaluated by considering the relationship confirmed by Gough and Pollard between t_{-1} and f_{-1} such as $\frac{t_{-1}}{f_{-1}} = \frac{1}{\sqrt{3}}$ then, $t_{-1} = \frac{f_{-1}}{\sqrt{3}}$

3) f_0 is fatigue limit in repeated axial loading can be found by using Haigh diagram of the material.

❖ Goodman equation:

$$\frac{\sigma_a}{\sigma_e} + \frac{\sigma_m}{\sigma_{ut}} = 1 \quad (2.8)$$

where:

- σ_a is the stress amplitude
- σ_m is the mean stress
- σ_e fatigue limit for completely reverse loading, can be assumed as $\sigma_e = 0.5 * \sigma_{ut}$
- σ_{ut} is ultimate tensile stress of the material

➤ Now, Goodman equation can be written as:

$$\sigma_e = 0.5 * (\sigma_{ut} - \sigma_m) \quad (2.9)$$

➤ And,

$$\sigma_e = \sigma_m \quad (2.10)$$

From equation (2.9) and (2.10), we can define:

$$f_0 = 0.34 * \sigma_{ut} \quad (2.11)$$

- 4) t_0 can be evaluated by considering the relationship confirmed by Gough and Pollard between t_{-1} and f_{-1} such as $\frac{t_0}{f_0} = \frac{1}{\sqrt{3}}$ then, $t_0 = \frac{f_0}{\sqrt{3}}$.
- 5) C_a shear stress on the examined plane. For our model the examined plane will be the critical plane. Critical plane approaches are useful methods when designing against long-term fatigue of machine components made from metals. The values of C and N has been found through MATLAB code, but then those values were used directly in the same script to find the maximum damage factor.

2.2.2 Findley Criterion:

This criterion proposed a linear combination of the maximum normal stress and the shear stress amplitude on the critical plane for a given number of cycles to failure N_f .

$$a_F C_a + b_F N_{max} \leq f_{-1} \quad (2.12)$$

where,

- $a_F = 2 \sqrt{\kappa - 1}$
- $b_F = 2 - \kappa$
- C_a is the shear stress on an examined plane (MPa)
- f_{-1} is fatigue limit in fully reversed axial loading (MPa)
- N_{max} is the maximum normal stress on examined plane (MPa)
- κ is fatigue limit ratio: $\kappa = \frac{f_{-1}}{t_{-1}}$ [-]

and indices,

- a: amplitude
- m: mean value

The critical plane orientation coincides with the plane orientation where the maximum value of this linear combination occurs.

- f_{-1} can be considered: $f_{-1} = \frac{R_m}{2}$, where R_m is ultimate tensile strength of the material.
- t_{-1} can be evaluated by considering the relationship confirmed by Gough and Pollard between t_{-1} and f_{-1} such as $\frac{t_{-1}}{f_{-1}} = \frac{1}{\sqrt{3}}$ then, $t_{-1} = \frac{f_{-1}}{\sqrt{3}}$.
- C_a shear stress on the examined plane. For our model the examined plane will be the critical plane. Critical plane approaches are useful methods when designing against long-term fatigue of machine components made from metals. According to Findley, the critical plane is one onto which the linear combination of shear stress amplitude and the maximum normal stress reaches its maximum value. The values of C_a and N_{max} has been found through MATLAB code, but then those values were used directly in the same script to find the maximum damage factor.

Critical Plane approach:

An approach that has been used in the First script formulas to evaluate high-cycle fatigue behaviour which relies on the determination of the amplitude and mean value of the normal and shear stresses acting on a particular plane (i.e in our case is also called critical plane).

Critical plane approaches are useful methods when designing against long term fatigue of machine components made from metals. According to Findley, the critical plane is the one onto which the linear combination of the shear stress amplitude and the maximum normal stress reaches its maximum value. Application of critical-plane type approaches to the evaluation of high-cycle fatigue behaviour relies on the determination of the amplitude and mean value of the normal and the shear stresses acting on a particular plane. The evaluation of the mean value and the amplitude of the normal stress acting on a given plane is a simple problem, because during each load cycle, the normal stress varies in magnitude but not in direction. The situation is more complex and complicated when it is shear stress because it varies both in magnitude and direction during each load cycle. As discussed in the article “Critical plane approaches in high-cycle fatigue: on the definition of the amplitude and mean value of the shear stress acting on the critical plane” that the Minimum-Circumscribed Circle method provides the better solution.[10]

Statement of the problem: By considering a material point of a body which is submitted to a cyclic loading and a material plane represented by Δ , passing through the point under consideration.[10]

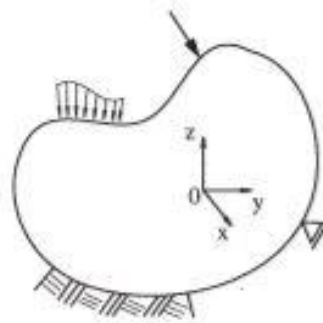


Figure 8 A body submitted to cyclic loading^[10]

The plane Δ is located by its unit normal vector \mathbf{n} , which is described by its spherical angles (ϕ, θ) . On the critical plane Δ the stress vector $\mathbf{S}_n = \boldsymbol{\sigma} \cdot \mathbf{n}$ is acting. This \mathbf{S}_n vector can be decomposed into two vectors, one is tangential to Δ , which is the shear

stress τ and one is perpendicular to the plane Δ , which is the normal stress σ_n . The projection of S_n on n is normal stress vector σ_n and can be defined as:

$$\sigma_n = (S_n \cdot n)n \Rightarrow \sigma_n = (n \cdot \sigma \cdot n)n \quad (2.13)$$

The shear stress τ can be defined as the difference of vector S_n and σ_n :

$$\tau = S_n - \sigma_n \Rightarrow \tau = \sigma \cdot n - (n \cdot \sigma \cdot n)n \quad (2.14)$$

This means that the shear stress vector τ is the orthogonal projection of the stress vector S_n onto the plane Δ . [10]

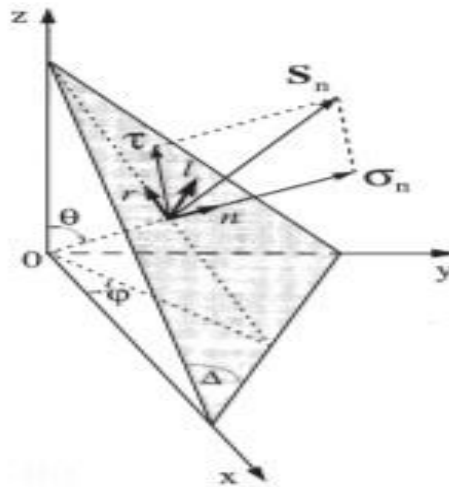


Figure 9 The projection of S_n on n is the normal stress vector [10]

During a complex cyclic loading, the tip of the stress vector S_n describes a closed space curve Φ as shown in figure below. [10]

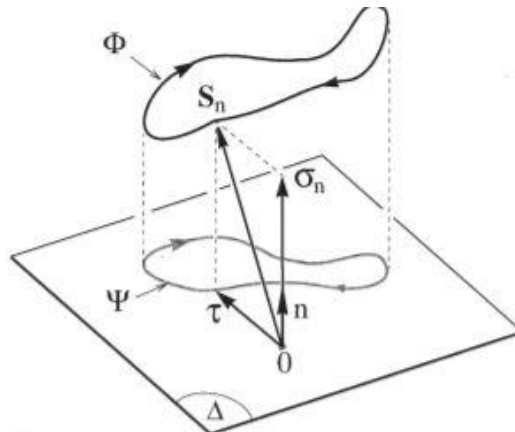


Figure 10 A closed space curve described by S_n [10]

As the normal stress vector σ_n conserves its direction invariant means its tip oscillates or changes between two points on the line defined by \mathbf{n} , and these two points are the extremes of the projection of the curve Φ onto \mathbf{n} . That's why, during a cycle of complex periodic load, σ_n changes only in magnitude but not in direction. The semi-difference between the maximum and minimum values that the function achieves during a load cycle provides its amplitude, whereas the semi-sum yields its mean value [10]:

$$\begin{aligned}\sigma_{n,a} &= \frac{1}{2} \left(\max_t (\mathbf{n} \cdot \boldsymbol{\sigma}(t) \cdot \mathbf{n}) - \min_t (\mathbf{n} \cdot \boldsymbol{\sigma}(t) \cdot \mathbf{n}) \right) \\ \sigma_{n,m} &= \frac{1}{2} \left(\max_t (\mathbf{n} \cdot \boldsymbol{\sigma}(t) \cdot \mathbf{n}) + \min_t (\mathbf{n} \cdot \boldsymbol{\sigma}(t) \cdot \mathbf{n}) \right)\end{aligned}\tag{2.15}$$

To find the amplitude and mean value of the shear stress is much more complex, because unlike normal stress vector σ_n , the shear stress vector changes both in direction and in magnitude inside each load cycle. During load cycle, the tip of shear stress vector describes a closed curve on Δ as shown in figure 10 above. At the end, $\boldsymbol{\tau}$ is vectorial periodic function of time. The curve Ψ described by $\boldsymbol{\tau}$ is different on different planes passing through the point under consideration. Therefore, the shear stress amplitude τ_a depends on the orientation of the plane on which it acts, i.e., it is a function of \mathbf{n} or equivalent function of ϕ and θ , i.e. $\tau_a(\phi, \theta)$. To find the maximum shear stress amplitude, $\max \tau_a$, one has to take into account all the planes passing through the point under consideration. This can be done by searching the maximum of τ_a over the angles ϕ and θ :

$$\max \tau_a = \max \{ \tau_a(\phi, \theta) \}\tag{2.17}$$

And now in order to find τ_a and τ_m on a given material plane Δ , there has been used Minimum Circumscribed Circle method which is the best proposal among others as mentioned in article above.[10]

Minimum-Circumscribed Circle Method:

By assuming that mean shear stress vector τ_m has been located on the material plane Δ and then the amplitude of the shear stress vector τ_a is equal to the length of the segment that joins the tip of the vector τ_m to the most distant point on the curve Ψ . In order to locate τ_m it is proposed to take as the vector that points to centre of the minimum circle circumscribed to the curve Ψ . The shear stress amplitude on the plane Δ is then equal to the radius of this circle. [10]

Consider a plane Δ and compute $\boldsymbol{\tau}$ on this plane at finite number of instants $t_i = 1, 2, 3, \dots, m$ of the load period. The set $\boldsymbol{\tau}(t_i)$ is formed and the curve Ψ described by

τ on Δ is approximated by a polygon P of m vertices. By increasing m, one can make the polygon P be as close to the curve Ψ as one wishes. There are infinitely many circles that can be drawn on Δ to contain at their interior the polygon P. The smallest one of these circles, determines the mean stress τ_m on the plane Δ . The problem can be represented mathematically like this:

$$\tau_m = \min_w \left\{ \max_{t_i} \|\tau(t_i) - w\| \right\} \quad (2.18)$$

where w is a point on the plane Δ and $\tau(t_i)$ is an element of the set of m vertices of P. [10]

For example: assume that one arbitrarily chooses a point w' on Δ , the number of circles drawn with the centre in w' and containing the polygon P is still infinite. The smallest of these circles can be determined. Its radius is equal to the longest line segment, among the line segments joining w' and circumscribing P. Therefore, for a given w' the radius R' of the smallest circle entered on w' and circumscribing P is equal to:

$$R' = \max_{t_i} \|\tau(t_i) - w'\| \quad (2.19)$$

The relationship above mentioned is for the maximizing part of min-max problem given by equation. The minimizing part of this equation can be determined as follows. After having found the smallest circumscribed circle entered on a candidate centre w' , and one choose another candidate centre w'' leading to a circle always containing P, but now with radius R'' smaller than the R' as shown in figure below. In other words, one is looking to minimize the quantity $(\max_{t_i} \|\tau(t_i) - w'\|)$ by varying w . [10]

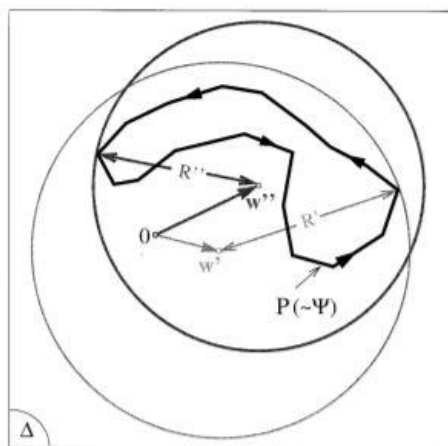


Figure 11 Minimum Circumscribed circle example [10]

This method is based on the theorem: *the minimum-circumscribed circle to plane polygon P is: either one of the circles drawn with a diameter equal to a line segment joining any two vertices of P or one of the circumcircles of all triangles generated from every three vertices of P.* [10]

The number n_D of line segments defined by any two vertices of P is equal to the number of combinations of m vertices of P taken two at a time,

$$n_D = \binom{m}{2} \Rightarrow n_D = \frac{m!}{2!(m-2)!} \quad (2.20)$$

whereas the number n_T of all triangles that can be generated combining every three vertices of P is equal to the number of combinations of m taken three at a time:

$$n_T = \binom{m}{3} \Rightarrow n_T = \frac{m!}{3!(m-3)!} \quad (2.21)$$

The steps to find the minimum-circumscribed circle to plane polygon P will be these:

- a) Assembled the set of line segments that formed by every two vertices of P. Number of elements of this set is equal to n_D . For each line segment, which is a side or chord of P, a circle is drawn with a diameter of the line segment under consideration. [10]
- b) The set of all the triangles generated from every three vertices of P is built. The number of the triangles denoted by n_T . For each triangle the circumcircle is drawn. [10]
- c) For each circle, among the $n_D + n_T$ circles drawn in previous steps, a check is performed to find out whether this circle contains the whole polygon P, which can be done by calculating the distances from the centre of this circle to all the vertices of P. If all the distances are smaller than or equal to the radius of the circle under consideration, the circle obviously circumscribes the polygon P. For such a circle, the coordinates of its centre and the length of its set can be denoted as C. [10]
- d) The elements of set C are all circles that contain the polygon P. According to the theorem, the circle with the smallest radius among the elements of set C is minimum-circumscribed circle to the polygon P. [10]

2. Correlation between oil debris amount and failure mechanism

Once the centre τ_m of the minimum-circumscribed circle to the curve Ψ has been found, the mean value and amplitude of the shear stress acting on Δ are given by:

$$\tau_m = \|\tau_m\|, \text{ and } \tau_a = \max_{t_i} \|\tau(t_i) - \tau_m\| \quad (2.22)$$

This method is a valuable method for computing the mean value and amplitude of the shear stress acting on a given plane Δ . [10]

First Matlab Script:

Part a: Contact pressures computation

Here the code has written in Matlab to find distribution of contact pressures when two spheres of the same material and geometry brought into contact is calculated.

The code in this script is based on the article “*Numerical solution of smooth and rough contact problems, Francesco Marmo, Ferdinando Toraldo, Alessandro Rosati*”.

Contact between two elastic bodies is an imperative problem from point of view of both solid mechanics and materials science. Contact occurs in several mechanical components such as gears, bearings, cam and follower, wheel, and rail for which contact fatigue is considered as one of the main causes of failure. As well it is known, the problem of contact between smooth elastic bodies under normal loading was first investigated by Hertz. In his original paper Hertz considered the contact between two dissimilar ellipsoids by approximating the geometry as the contact of the two half-spaces whose mismatch was assumed to be of elliptical shape and its dimension small when compared with the radius of curvature of the paraboloids. The 3D problem was solved by Hertz for a restricted class of the surfaces that are quadratic i.e. represented by a second-degree polynomial near the contact point. “*Hertz H (1882) On the contact of elastic solids. J. Reine und Angewandte Mathematik 92, 156–171*”. [11]

It is more convenient to exploit the so called semi-analytical or semi-numerical approach for non-conforming bodies, i.e., when the characteristic size of the contact surface is small compared to those of the contact bodies. The semi-analytical approach is basically based on the discretization of the integral equation governing the local contact problem. In order to reduce drastically the computational time associated with the evaluation of the exact values of the surface displacement induced by a pyramidal distribution of the normal and tangential contact pressures, the analytical solutions have been replaced by the approximated solutions. Approximated surface displacements have been determined numerically by tuning the scalar coefficients multiplying the characteristic dimension of the hexagonal base of the pyramidal load function and the distance between the field point and the centre of the pyramid. [11]

Non-Conforming smooth bodies contact:

By considering two isotropic elastic non-conforming smooth bodies in contact, as shown in figure 12, the x-y plane is assumed to be tangent to the surfaces of both the bodies at the point of first contact P while z is the orthogonal to such a plane.

Because of the effect of some external actions, both bodies deform in the vicinity of P in such a way that they touch over a surface where contact pressures are transmitted between the bodies. [11]

According to Hertz theory, if the characteristic length of the region of contact is small with respect to the characteristic length of both bodies and with respect to the curvatures of both bodies' surfaces, the contact problem can be solved by modelling both bodies as isotropic half-spaces, whose free surface lies on the x-y plane.

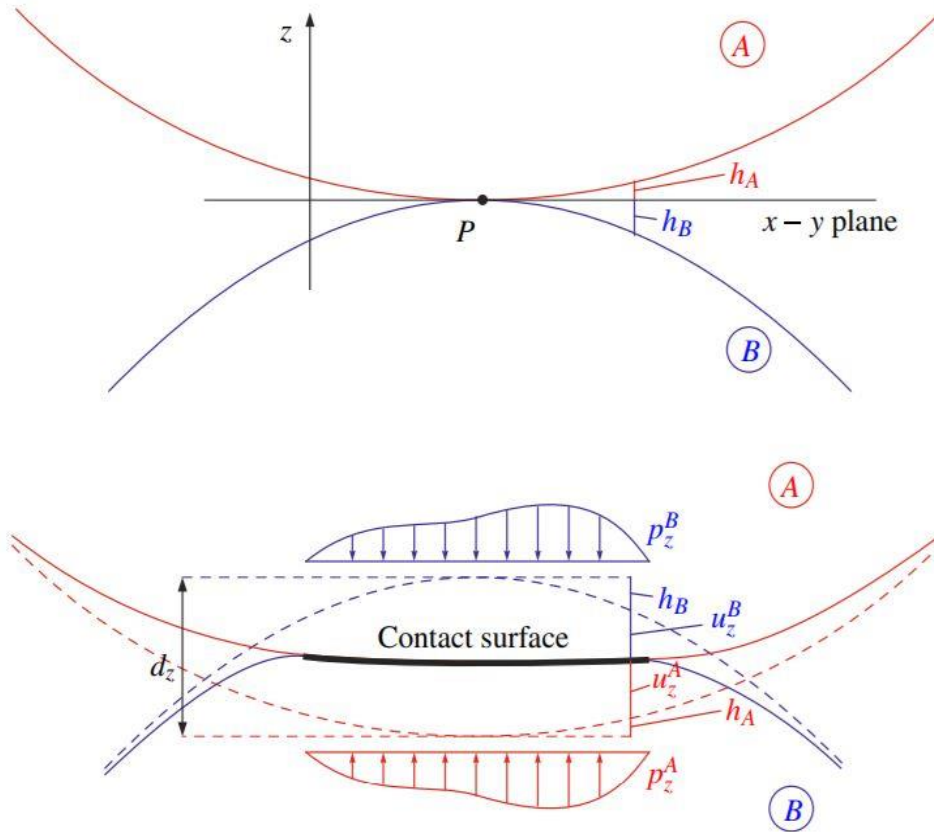


Figure 12 2-D schematic representation of the contact between non-conforming smooth bodies [11]

$h_A(x,y)$ and $h_B(x,y)$ are the profiles of the two bodies, defined as the z coordinate of the points of bodies' surfaces, $u_z^A(x,y)$ and $u_z^B(x,y)$ are the vertical displacements the bodies' surfaces and the vertical displacement can be calculated as $d_z = d_z^A - d_z^B$ between two far points always the parts of the bodies, related by the compatibility condition:

$$h_A(\rho) + u_z^A(\rho) - h_B(\rho) - u_z^B(\rho) = d_z \quad (2.23)$$

where $\rho(x,y)$ are the true points belonging to the contact surface. Outside the surface of contact, as compenetration of the two bodies is not allowed so right-hand side of the compatibility equation cannot be greater than the left-hand side, while the

opposite condition can be taken place where left hand side of the equation is greater than left hand side.[11]

When the contact is adhesive, the compatibility condition equation (2.23) is strengthened by also including the horizontal component of displacements, by means of conditions (2.12) holding only for the points within the contact surface.

$$u_x^A(\rho) - u_x^B(\rho) = d_x \quad \text{and} \quad u_y^A(\rho) - u_y^B(\rho) = d_y \quad (2.24)$$

Displacements u_j^A and u_j^B where $j = x, y, z$ are function of the contact normal pressures $p_z^A(x, y) = -p_z^B(x, y) = p_z(x, y)$ and in the case of adhesive contact displacements are also function of the tangential pressures $p_x^1(x, y) = -p_x^2(x, y) = p_x(x, y)$ and $p_y^A(x, y) = -p_y^B(x, y) = p_y(x, y)$. Here p_k^B represents the pressure exerted by the body A on the body B along the direction $k = x, y, z$ and p_k^A in the similar manner.[11]

2. Displacements induced by arbitrary distributions of pressures:

Points lying within the contact surface, can be enforced by the conditions (2.23) and (2.24), but in order to do that, formulas are required which can evaluate the displacement field generated by the arbitrary distributions of the pressures. As depicted by the Hertz theory, local effects of contact can be evaluated by employing available solutions for isotropic elastic half-spaces loaded on their surface by the contact pressures. The surfaces of the two bodies in contact are discretized around P by means of a mesh composed of vertices V and non-overlapping triangles T connecting triplets of vertices. Accordingly, values of pressure $p_j(\rho_i^a) = p_j(x_i^a, y_i^a)$, $i=1,2,3$ and $j = x, y, z$, that are associated with the vertices $\rho_i^a = (x_i^a, y_i^a)$ of the generic triangle a of the mesh, interpolate the actual pressure as shown in figure below.[11]

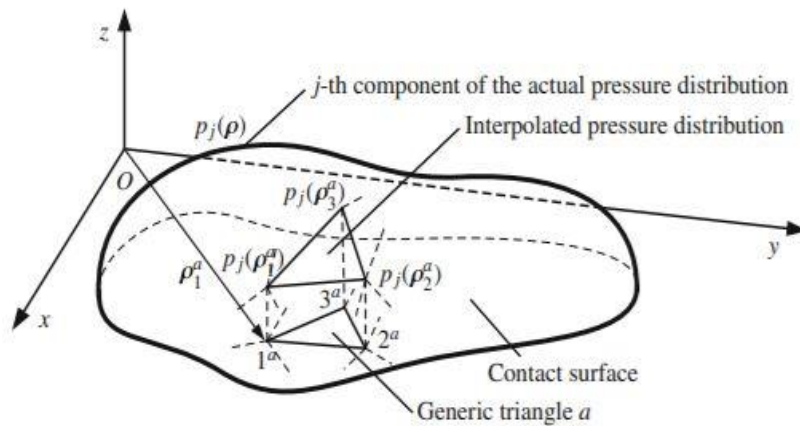


Figure 13 Interpolation of the pressure distribution by a triangular mesh [11]

In particular each triangle of the mesh has load parameters p_{0j}^a , p_{1jx}^a and p_{1jy}^a and can be evaluated by solving three systems of equations of such kind:

$$p_{0j}^a + p_{1jx}^a x_i^a + p_{1jy}^a y_i^a = p_j(\rho_i^a), \quad i=1,2,3 \quad (2.25)$$

Equation (2.13) is relevant to each component $j = x, y, z$ of the contact pressure. These systems of equation can be solved in the matrix form:

$$\begin{pmatrix} p_{0j}^a \\ p_{1jx}^a \\ p_{1jy}^a \end{pmatrix} = \begin{pmatrix} 1 & x_1^a & y_1^a \\ 1 & x_2^a & y_2^a \\ 1 & x_3^a & y_3^a \end{pmatrix}^{-1} \begin{pmatrix} p_j(\rho_1^a) \\ p_j(\rho_2^a) \\ p_j(\rho_3^a) \end{pmatrix}$$

The horizontal displacements are indicated by $u_h^a = (u_x^a, u_y^a)$ and the vertical displacements are indicated by u_z^a , these displacements are induced by the generic a -th triangle of the mesh and u_h^a, u_z^a can be defined as[11]:

$$u_h^a(x, y) = \frac{1}{4\pi z} [(1 - 2\nu)(s_g'^a p_{0z}^a + S_{g\rho}'^a p_{1z}^a) + 2(s''^a p_{0h}^a + P_{1h}^a s_\rho''^a) + 2\nu(S_H^a p_{0h}^a + S_{H\rho}^a p_{1h}^a)] \quad (2.26)$$

$$u_z^a(x, y) = \frac{1}{4\pi z} [2(1 - \nu)(s''^a p_{0z}^a + s_\rho''^a p_{1z}^a) + (1 - 2\nu)(s_g'^a p_{0h}^a + S_{g\rho}'^a p_{1h}^a)] \quad (2.27)$$

where G is the shear modulus and ν is the Poisson ratio. The quantities $S_{(\cdot)}^{(\cdot)a}$ are tensors of second and third order and represent area integrals extended to the generic triangle a . For the sake of the simplicity the explicit depends upon the variables x and y , what characterizes the quantities $s_g'^a, S_{g\rho}'^a, s''^a, S_H^a, S_{H\rho}^a$ has been omitted.[11]

The displacement field induced by all pressure distribution $p(\rho) = (p_z^a, p^a(\rho))$, $a \in T$, and ρ belong to the contact surface, is obtained by the superposition of the displacements induced by the all the n triangles of the mesh. And u_i provides the displacement field induced by a given pressure distribution and it can be written as:

$$u_i = \sum_{a=1}^n u_i^a, \quad i = x, y, z \quad (2.28)$$

The resultant $f = (f_x, f_y, f_z)$ of the pressure function $p(\rho)$ is estimated by recalling that the interpolated pressure distribution is linear on each triangle; so, we have

$$f_j = \frac{1}{3} \sum_{a=1}^n A_a (p_j(\rho_1^a) + p_j(\rho_2^a) + p_j(\rho_3^a)) \quad (2.29)$$

where A_a is the area of triangle a and its evaluated as function of the position of its vertices by following the well-known formula [11] :

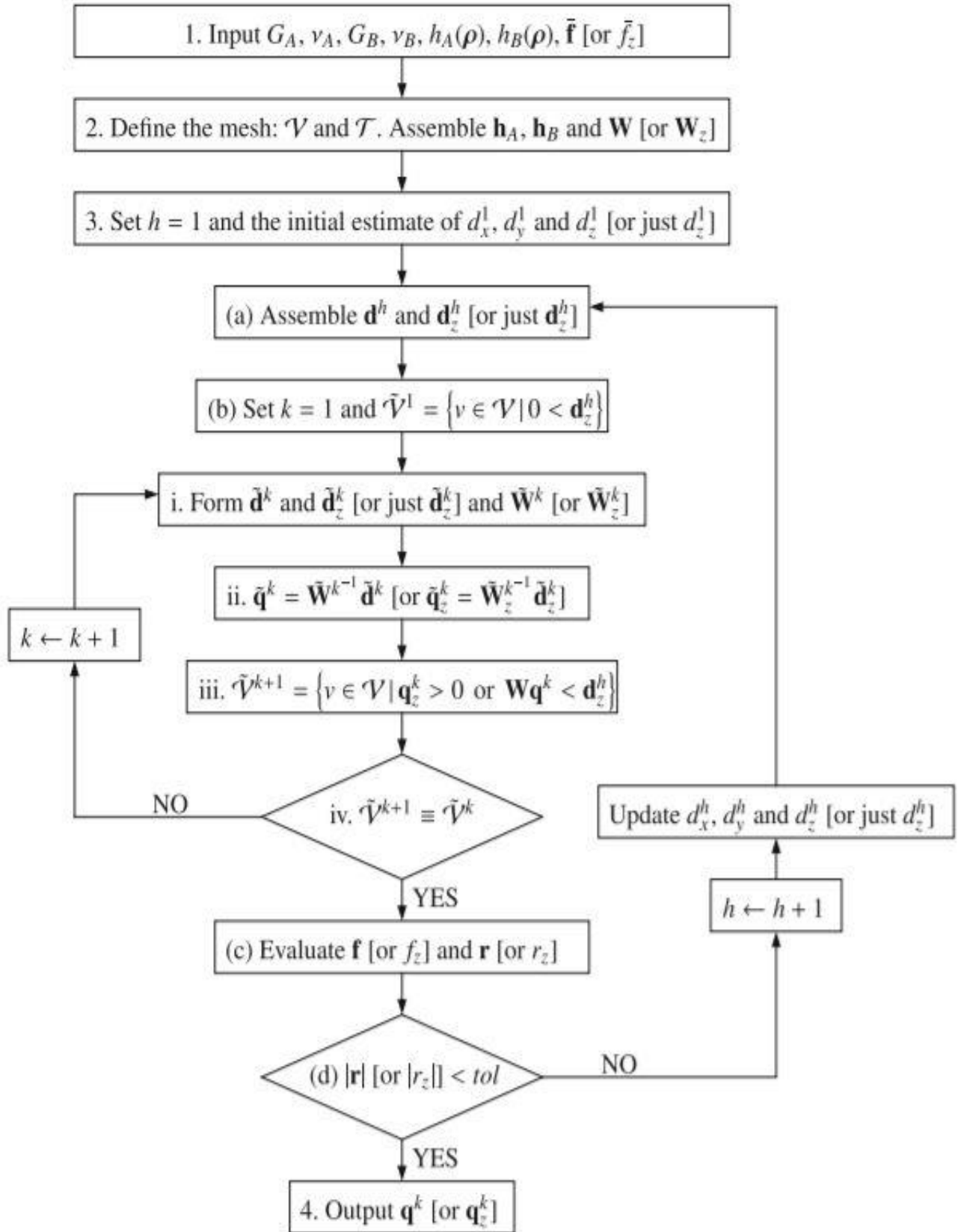
$$A_a = \frac{1}{2} \sum_{v=1}^3 \rho_v^a \cdot \rho_{v+1}^{a\perp} \quad (2.30)$$

And where it is assumed $\rho_4^a = \rho_1^a$ and $\rho_v^{a\perp} = (y_v^a, -x_v^a)$

Discrete compatibility equations:

The displacement field given by the formulas (2.26), (2.27), (2.28) can be used to enforce the compatibility conditions at any desired point of the contact surface. These conditions need to rewrite to evaluate the unknown contact pressures in such a way to make explicit the dependence upon the values obtained by the function $p(\rho)$ at the vertices of the triangular mesh. This has been done considering the interpolation of the pressure distribution shown in figure 9, as a superposition of pyramidal pressure distributions. In particular, each pyramid is a superposition of the load functions defined on the set of the triangles that share the same vertex.[11]

Matlab script has been written on the basis of iterative procedure for solving adhesive and smooth contact problems by following these steps:



The steps can be summarized as follows:

1 Input the material properties such as shear modulus, Poisson's ratios: G_A , ν_A , G_B , ν_B of the two bodies in contact, the profiles of their surfaces $h_A(\rho)$ and $h_B(\rho)$ and the external force vector $\bar{\mathbf{f}}$ exerted between the two bodies i.e., the resultant vector of the contact pressure distribution to be determined.[11]

2. Then in second step there has been defined a triangular mesh the surface of the two bodies, where the mesh is assigned as a set V of nodes, having position ρ_v , and a set T of non- overlapping triangles connecting triplets of the nodes. Once the mesh is defined it is possible to assemble the vectors \mathbf{h}_A and \mathbf{h}_B collecting the values of the surface profiles at the nodes of the mesh, and the matrix W collecting the difference between the surface normal displacements induced by unitary pyramidal (functions having a regular hexagon as a base and known values at the vertices of a reference mesh assigned over the potential contact region) load distribution.[11]

3. In this step an initial estimate of d_x^1 , d_y^1 and d_z^1 of the relative displacements d_x^h , d_y^h , and d_z^h between far points of the two bodies, here far points considered the points that are far from the area of contact were set. Then a series of the iterations were computed to correct such an estimate so as to fulfil equilibrium with applied contact forces This first order of iterations is subdivided into the following steps [11]:

a) First collect the vectors \mathbf{d}^h , \mathbf{d}_z^h as a function of the current estimate of the relative displacements between far points.[11]

b) In both the cases adhesive or smooth contact, the estimated value of the \mathbf{d}_z^h is used to form the list \tilde{V} of nodes related to the contact region according to the condition $\tilde{V} = \{v \in V \mid 0 < \mathbf{d}_z^h\}$ that is the set of nodes for which the assigned values of \mathbf{d}_z^h correspond to compenetrations of the two bodies assumed to be the infinitely rigid. A nested iterative procedure is employed to evaluate the contact forces p^h [or f_z] corresponding to the current estimate of \mathbf{d}^h [11]:

i) Form the vectors $\mathbf{d}^{\tilde{h}}$ and $\mathbf{d}_z^{\tilde{h}}$ by selecting components of \mathbf{d}^h and \mathbf{d}_z^h corresponding to the nodes in $V^{\tilde{h}}$; form the matrix \tilde{W} by selecting the rows and columns of W corresponding to nodes in \tilde{V} .[11]

ii) Solve equation: $\tilde{W}\tilde{\mathbf{q}} = \tilde{\mathbf{d}}$ (where \tilde{W} is a square matrix of order $3\tilde{N}_v$ and $\tilde{\mathbf{d}}$ is the vector of \tilde{N}_v components. \tilde{N}_v are the nodes internal to the region of contact) in order to evaluate the load parameters relevant to the nodes within the contact region, i.e. $\tilde{\mathbf{q}} = \tilde{W}^{-1} \tilde{\mathbf{d}}$. Load parameters of nodes outside the contact region are set to zero.[11]

iii) Update the list of \tilde{V} of nodes pertaining to the contact region according to the condition: $\tilde{V} = \{v \in V \mid q_z > 0 \text{ or } \mathbf{W}\mathbf{q} < d_z\}$ i.e., by selecting of nodes at which the normal contact pressures are positive so compressive pressures or those corresponding to compenetration between the bodies in contact. [11]

iv) If the list \tilde{V} has changed with respect to the one estimated at step (a) or at the step iii) of the previous iteration then go back to step i); otherwise continue to step (c), and the step (c) is focused on evaluating the pressure resultant f^h by employing equation (2.17) and the residual $r^h = \frac{\bar{f}^h - f^h}{|\bar{f}^h|}$. [11]

d) If $|r^h| < \text{tol}$, go to step 4; otherwise update the estimate of d_x, d_y and d_z as:

$$d_i^{h+1} = d_i^h + \frac{d_i^h - d_i^{h-1}}{f_i^h - f_i^{h-1}} (\bar{f}_i - f_i^h), \quad i = x, y, z$$

and go back to the step (a). [11]

4.) The current estimate of displacements d_x^h, d_y^h , and d_z^h is in equilibrium with applied external loads \bar{f} ; hence the current value of the load parameters q^h interpolates the actual distribution of pressures and they can be used to evaluate all the desired mechanical fields within both bodies. [11]

By following this procedure and implementing this in Matlab code, distribution of contact pressures when two spheres of the same material and geometry brought into contact is calculated. Spheres radii have different values one is comparatively bigger than another one. Sphere with bigger radius is pushed towards another sphere by a force with a constant value. The x-y plane has been discretized by a mesh as shown in figure 14 below.

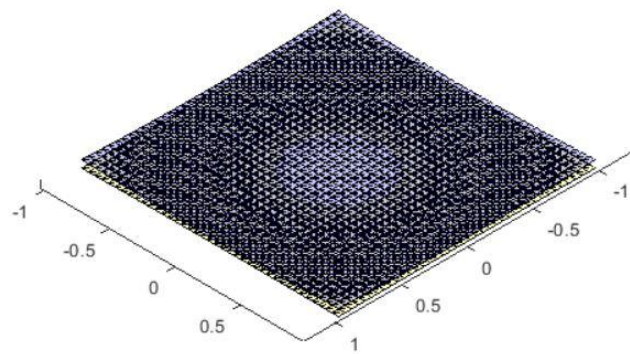


Figure 14 x-y plane discretized by a mesh

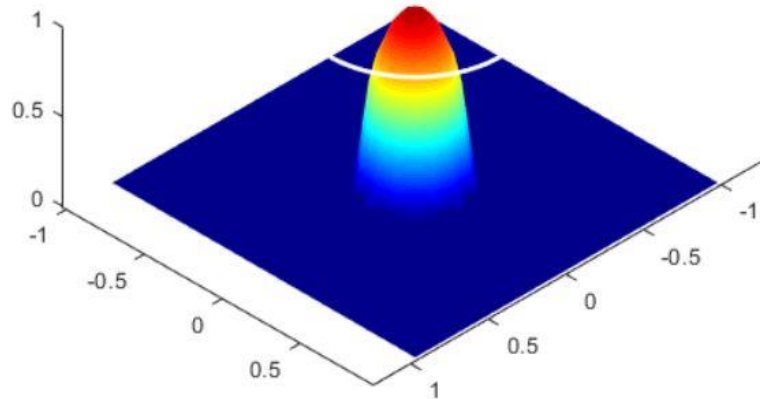


Figure 15 Distribution of contact pressures

Part b: Computation of stresses from the contact pressures

The procedure has been taken from the article “*A general approach to the solution of Boussinesq’s problem for polynomial pressures acting over polygonal domains, Francesco Marmo, Luciano Rosati.*” A general approach is outlined for extending the classical Boussinesq’s solution to the case of pressures distributed according to a polynomial law of arbitrary order over a polygonal domain. Analytical expressions of displacements, strains and stresses are derived at an arbitrary point of the half-space as a function of the loading function and of the position vectors.

Definition of the Problem:

Let us consider a linearly elastic half-space ($z \geq 0$) whose surface ($z = 0$) is traction free. A force $\mathbf{f} = (0, 0, f_z)^t$, orthogonal to the surface of the half-space, is applied at a point $F = (x', y', 0)^t$ as shown in figure below.[13]

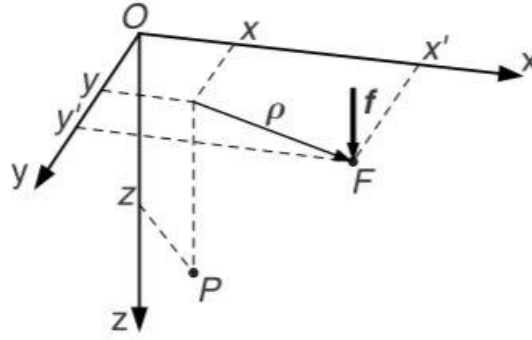


Figure 16 Vertical force applied to the surface of a half-space [13]

Point $P = (x, y, z)^t$ which denotes the coordinates of an arbitrary point within the half-space the displacements and stresses at P have been expressed by means of the potential function:

$$\phi(\rho, z) = z \log(z + \sqrt{\rho \cdot \rho + z^2}) - \sqrt{\rho \cdot \rho + z^2} \quad (2.31)$$

and where: $\rho = (x' - x, y' - y)^t$

The formulas to express the displacements associated with f_z :

$$\mathbf{u}_h^f(\rho, z) = \frac{f_z}{4\pi G} [(1 - 2\nu) \mathbf{grad}\phi' + \mathbf{grad}\phi''] \quad (2.32)$$

$$\mathbf{u}_z^f(\rho, z) = \frac{f_z}{4\pi G} [2(1 - \nu) \phi' + z \phi''] \quad (2.33)$$

where $\mathbf{u}_h = (u_x, u_y)^t$ is a vector collecting the horizontal components of the displacement. The elastic parameters G and ν represent the Poisson's ratio and the shear modulus of the half-space respectively, $\mathbf{grad} = (\partial/\partial x, \partial/\partial y)^t$ is the 2D gradient operator and

$$\phi'(\rho, z) = \frac{\partial \phi}{\partial z} = \log(z + \sqrt{\rho \cdot \rho + z^2}),$$

$$\phi''(\rho, z) = \frac{\partial^2 \phi}{\partial z^2} = \frac{1}{\sqrt{\rho \cdot \rho + z^2}},$$

$$\phi'''(\rho, z) = \frac{\partial^3 \phi}{\partial z^3} = \frac{1}{(\rho \cdot \rho + z^2)^{3/2}}$$

Denoting \mathbf{E} the infinitesimal strain tensor and $(\cdot)^T$ is the transpose operator:

$$\mathbf{E} = \begin{pmatrix} \varepsilon_x & \frac{1}{2}\gamma_{xy} & \frac{1}{2}\gamma_{xz} \\ \frac{1}{2}\gamma_{yx} & \varepsilon_y & \frac{1}{2}\gamma_{yz} \\ \frac{1}{2}\gamma_{zx} & \frac{1}{2}\gamma_{zy} & \varepsilon_z \end{pmatrix} = \begin{pmatrix} \mathbf{E}_h^f & \frac{1}{2}\boldsymbol{\gamma}_z^f \\ \frac{1}{2}\boldsymbol{\gamma}_z^{fT} & \varepsilon_z^f \end{pmatrix}, \quad (2.34)$$

And the \mathbf{E} splitting in the sub-tensors:

$$\mathbf{E}_h^f(\boldsymbol{\rho}, z) = \frac{f_z}{4\pi G} [(2\nu-1) \mathbf{H}(\phi') + \mathbf{H}(\phi'')], \quad (2.35)$$

$$\frac{1}{2}\boldsymbol{\gamma}_h^f(\boldsymbol{\rho}, z) = \frac{f_z}{4\pi G} z \mathbf{grad}\phi''', \quad (2.36)$$

$$\varepsilon_h^f(\boldsymbol{\rho}, z) = \frac{f_z}{4\pi G} [(1-2\nu) \phi' + z\phi^{iv}], \quad (2.37)$$

where $\mathbf{H}(\cdot) = \mathbf{grad grad}(\cdot)$ is two-dimensional Hessian Matrix of (\cdot) . Finally, the stress tensor is expressed as function of \mathbf{E} by the linear isotropic elastic law:

$$\mathbf{T} = 2G [\mathbf{E} + \frac{\nu}{1-2\nu} (\text{tr}\mathbf{E})\mathbf{1}] \quad (2.38)$$

where $\mathbf{1}$ is three-dimensional identity tensor.

Combining formulas (2.35) and (2.38), the stress tensor can be computed as:

$$\mathbf{T}_h^f(P) = \frac{f_z}{2\pi} [2\nu \phi''' \mathbf{1} + (2\nu-1) \mathbf{H}(\phi') + z \mathbf{H}(\phi'')], \quad (2.39)$$

$$\boldsymbol{\tau}_z^f(P) = \frac{f_z}{2\pi} z \mathbf{grad}\phi''', \quad (2.40)$$

$$\sigma_z^f(P) = \frac{f_z}{2\pi} [\phi''' + z\phi^{iv}], \quad (2.41)$$

where the stress tensor \mathbf{T} has been partitioned as \mathbf{E} in the form:

$$\mathbf{T} = \left(\begin{array}{cc|c} \sigma_x & \tau_{xy} & \tau_{xz} \\ \tau_{yx} & \sigma_y & \tau_{yz} \\ \hline \tau_{zx} & \tau_{zy} & \sigma_z \end{array} \right) = \left(\begin{array}{cc} \mathbf{T}_h^f & \tau_z^f \\ \tau_z^{fT} & \sigma_z^f \end{array} \right), \quad (2.42)$$

where \mathbf{I} is three-dimensional identity tensor.

Output:

- 1) The contact pressure of each element and position of the pitch.
- 2) Principal stresses ($\sigma_1, \sigma_2, \sigma_3$) of each element and position of the pitch.
- 3) Shear and normal stress ($\tau_x, \tau_y, \tau_z, \sigma_x, \sigma_y, \sigma_z$) of each element and position of the pitch.
- 4) Most importantly the stress tensor of each element and position of the pitch.

Second Matlab script:

This function takes input the stress tensor i.e., obtained from the first Matlab script mentioned above for each position and then this function provides alternate and mean stress as output for each position.

From stress underneath the surface, the alternate and mean stress can be computed of a single point in the pitch by using failure criterions as follows:

Formulas manipulated from PCr and Findley criterion to compute mean and alternate stress for each element and position:

PCr criterion:

$$\sigma_a = \sqrt{a_{PC} * C_a^2 + b_{PC} * N_a} ; \text{ alternate stress}$$

$$\sigma_m = \sqrt{b_{PC} * (d_{PC} * N_m)} ; \text{ mean stress}$$

Findley Criterion:

$$\sigma_a = a_F C_a ; \text{ alternate stress}$$

$$\sigma_m = b_F N_{max} ; \text{ mean stress}$$

Third Matlab script:

Then there is another script written in Matlab, which takes input as alternate and mean stress of each element and position computed from PCr and Findley criterion respectively and calculate number of cycles to failure in following steps:

- 1) Fatigue limit has been found by using following formula for each element and position:

$$\sigma_D = \frac{\sigma_{ut}}{2 + \sigma_m / \sigma_a} \tag{2.43}$$

where:

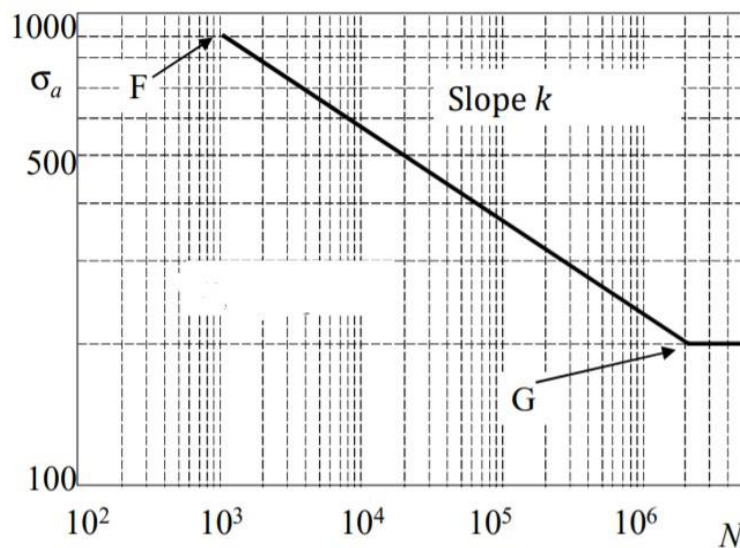
- σ_a is the stress amplitude
- σ_m is the mean stress
- σ_{ut} is ultimate tensile stress of the material

- 2) To find number of cycles to failure, Basquin equation has been used.

Basquin equation:

$$\sigma_a^k * N = \sigma_D^k * (2 * 10^6) \tag{2.44}$$

To find k we can use S-N diagram:



Therefore, points F and G have coordinates:

$$F: (N_F, \sigma_F) = (10^3, 0.9*(R_m - \sigma_{ut}))$$

$$G: (N_G, \sigma_G) = (2*10^6, \sigma_D)$$

$$k = \frac{\log(2*10^6) - \log(1000)}{\log(|0.9*(\sigma_{ut} - \sigma_m)|) - \log(\sigma_D)} \quad (2.45)$$

As, σ_m for each element and position at pitch line has different value, k also has different value for each element and position at the pitch line.

Number of cycles to failure for each position of the contact at the pitch:

$$N = \left(\frac{\sigma_D}{\sigma_a}\right)^k * (2 * 10^6) \quad (2.46)$$

And the damage factor can be computed as:

$$D = \frac{1}{N} \quad (2.47)$$

The damage factor that is considered for each contact position between pair of teeth is the maximum damage factor among the damage factor of each element for single position respectively.

3.Results Validation:

To select best criterion among PCr and Findley to find damage factor so number of cycles to failure for pitting:

3.2 Case 1- By using non-realistic values of contact pressures:

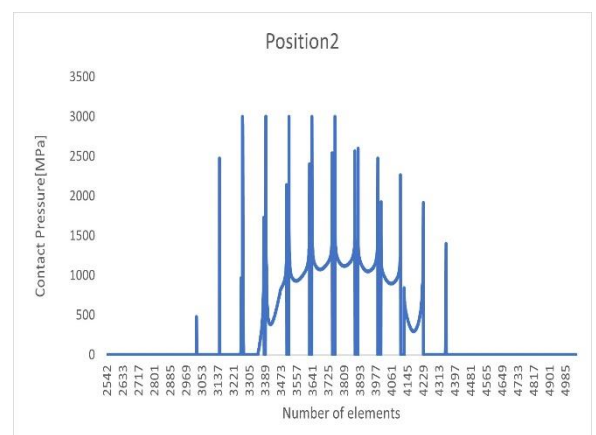
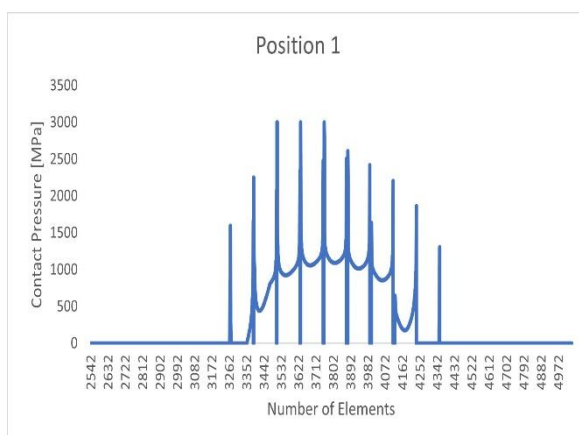
In this case the dimension of gears, are not near to the dimensions of gears we normally have in gearbox. So, the contact pressure between teeth of these are quite high. This case has been performed in order to do sensitivity analysis of both the failure criterions on the basis of contact pressure values. So, to see what results we get, or which criterion among these two reacts better to high pressure values.

Contact pressure has been evaluated for each element of the mesh of the contact area of the teeth. First, to check if both criterions give at least a reasonable value of damage factor, PCr and Findley criterion were analysed for only one contact position so, when the pair of teeth first comes in contact.

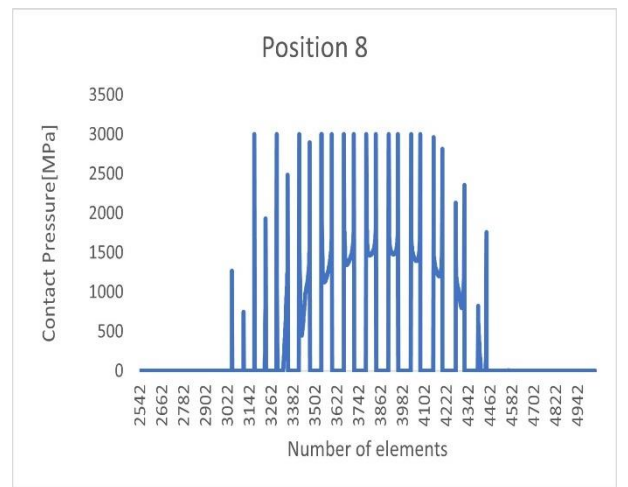
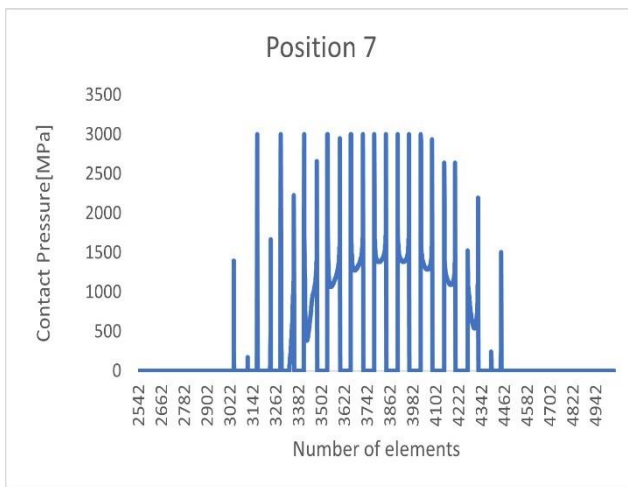
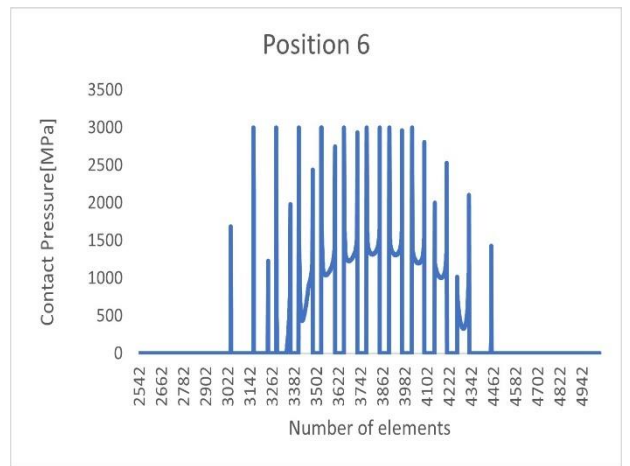
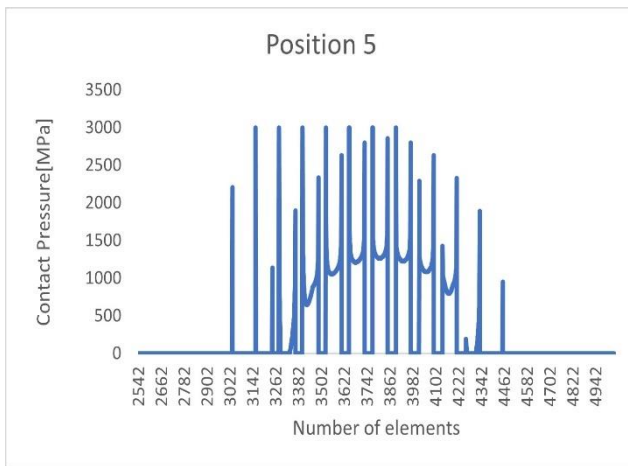
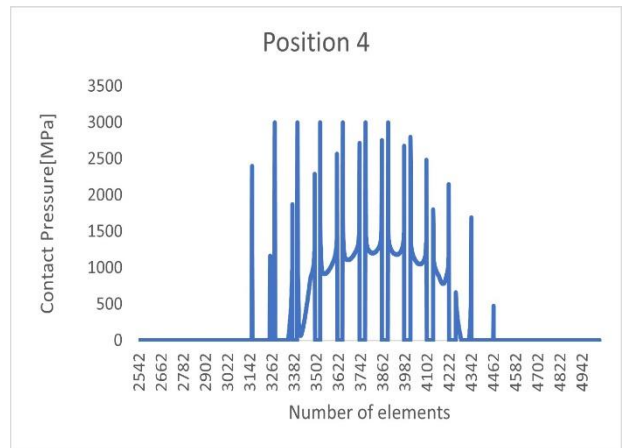
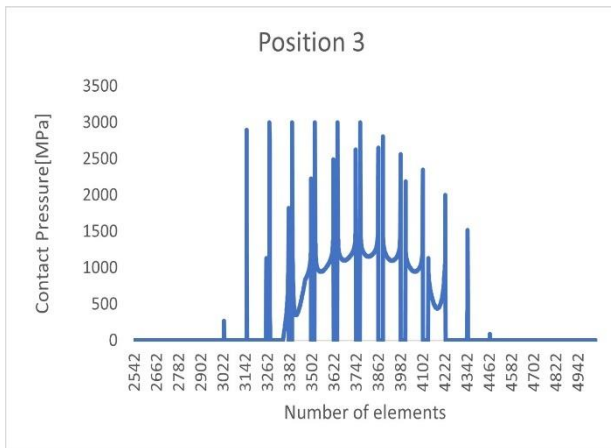
In order, to calculate number of cycles to failure or damage factor, both criterions must be analysed for all the position along the pitch. In this case total positions considered were 21 positions. Position here is referenced to the number of contacts among the pair of teeth.

By following semi-analytical method and approach mentioned in first Matlab script, contact pressures values has been computed for all pairs of teeth in contact, but for analysis only pair considered from 2542 to 5082 number of elements along the whole pitch line.

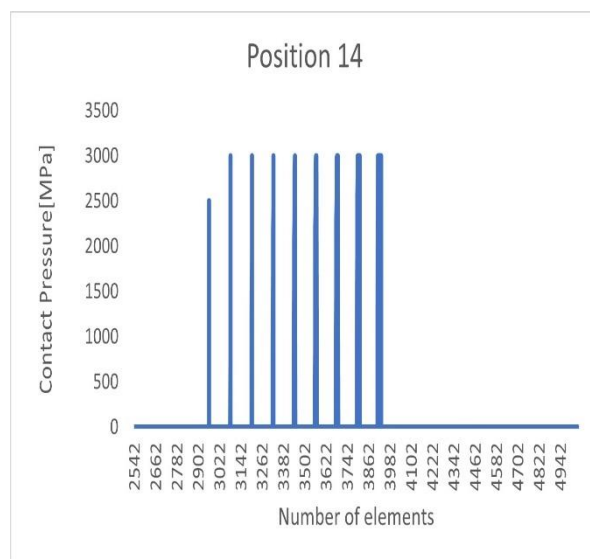
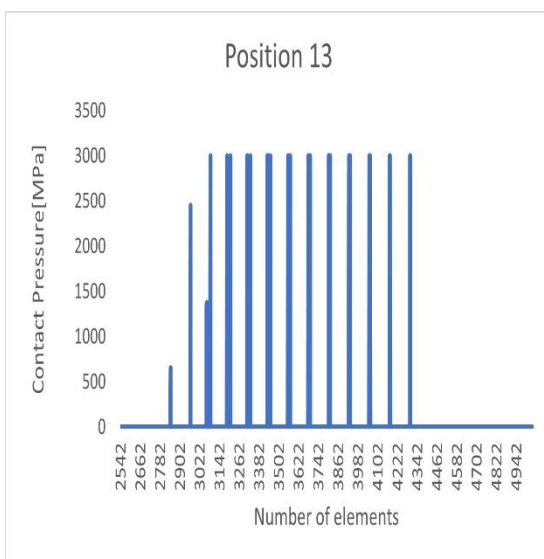
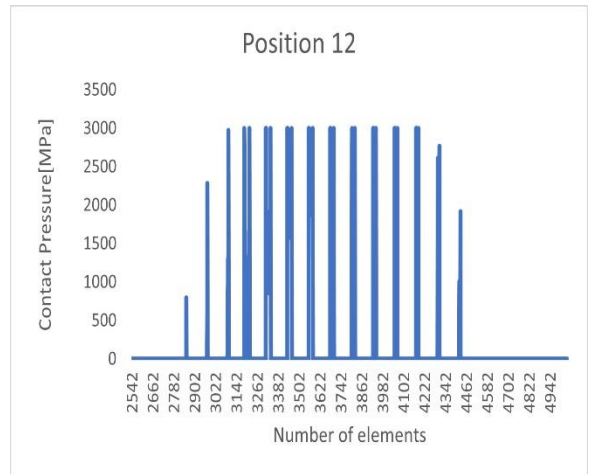
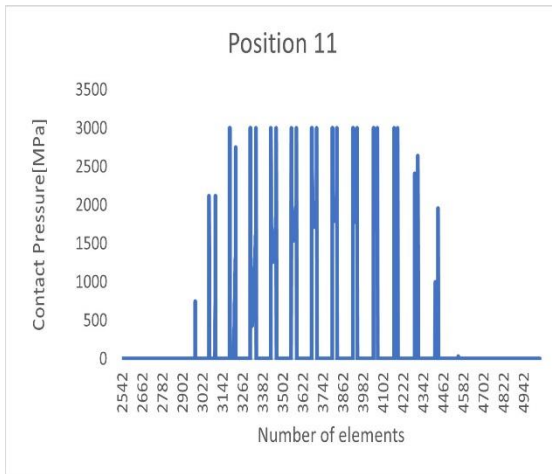
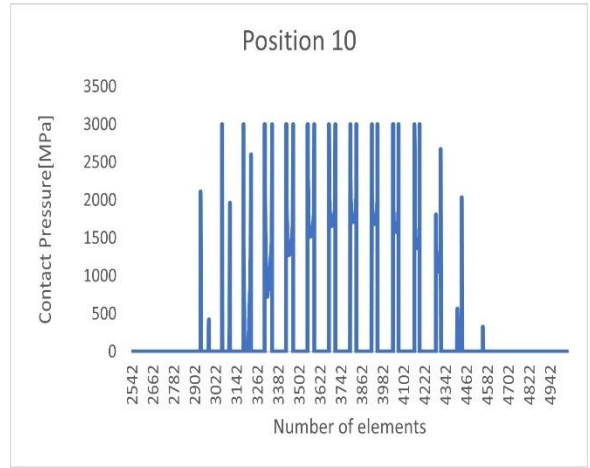
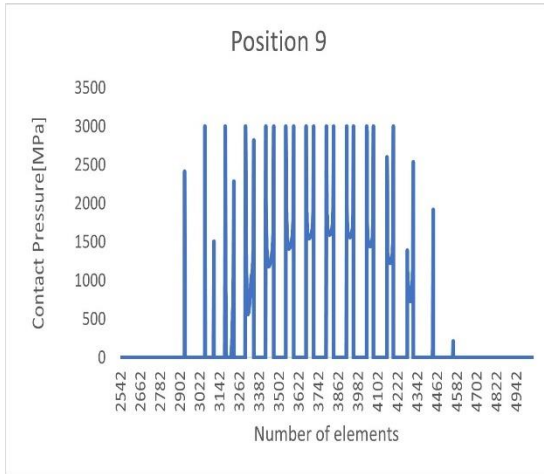
Pressure distribution for each position:



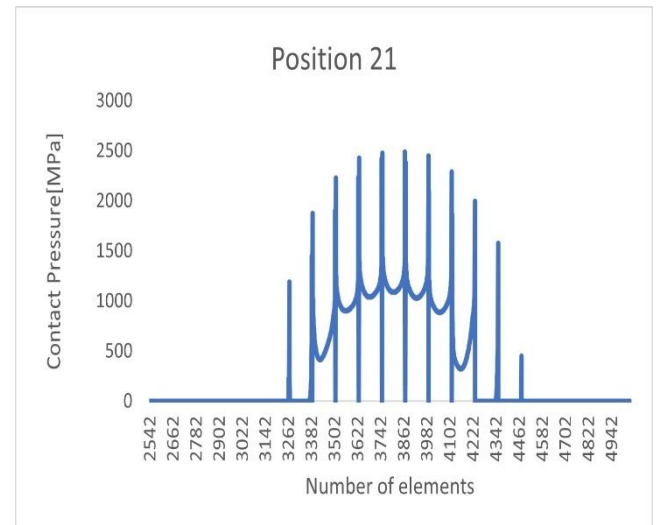
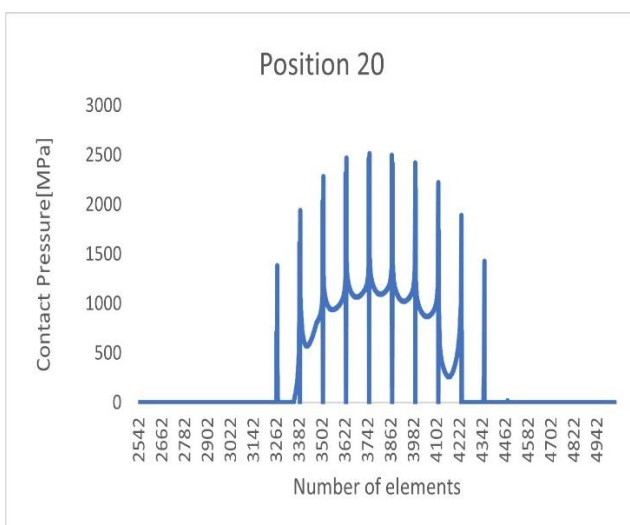
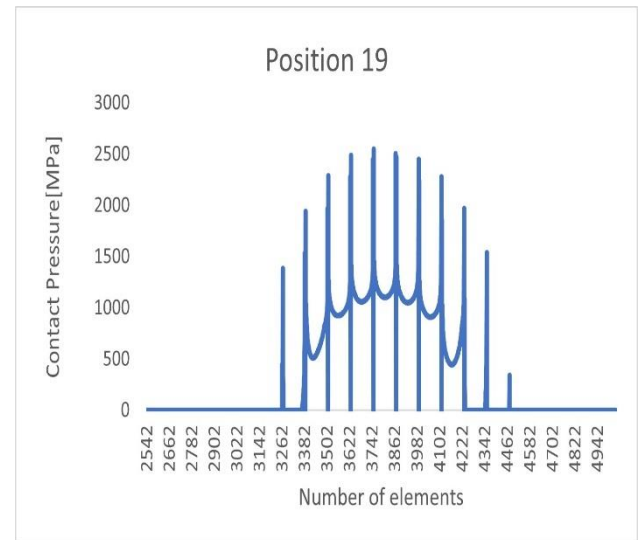
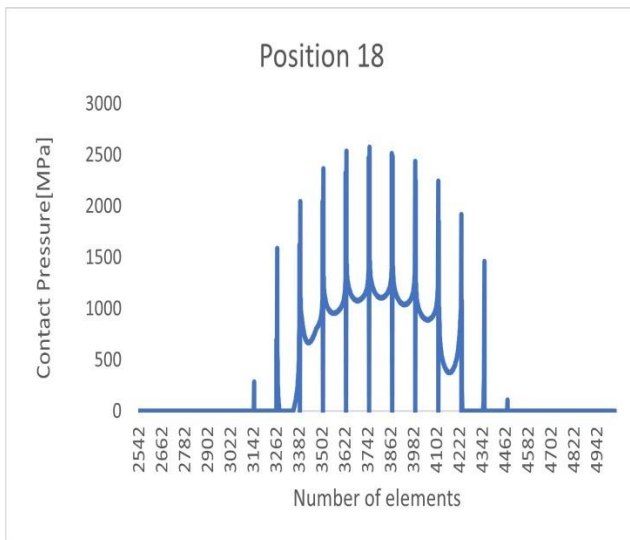
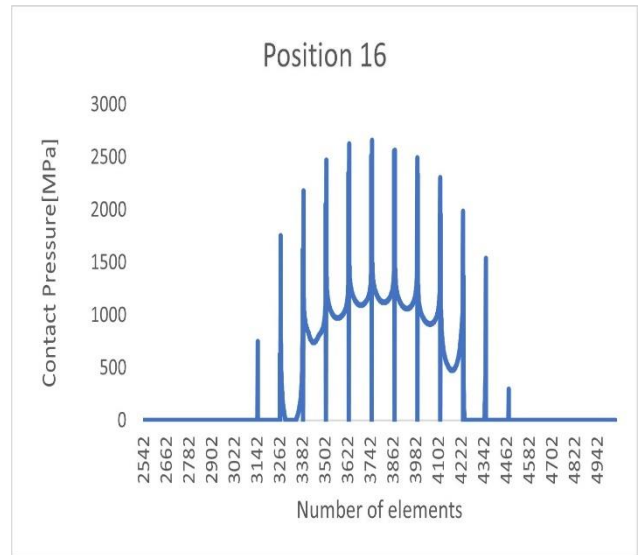
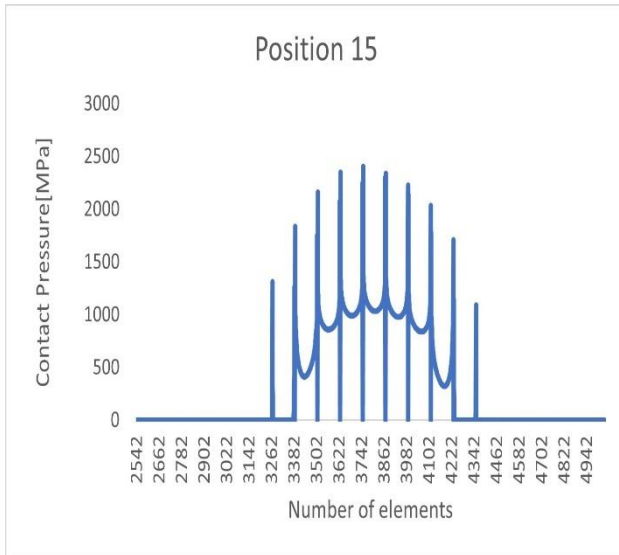
3.Results Validation:



3.Results Validation:



3.Results Validation:

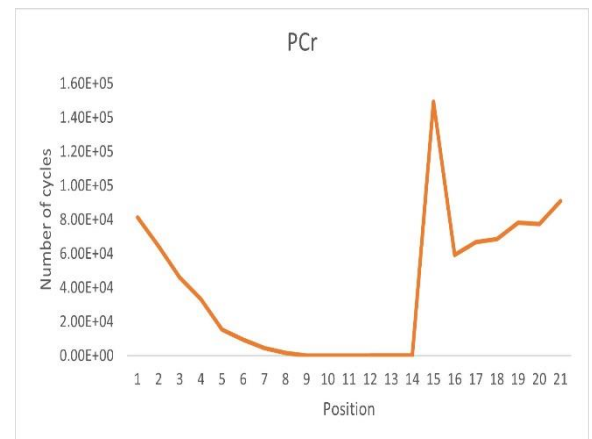
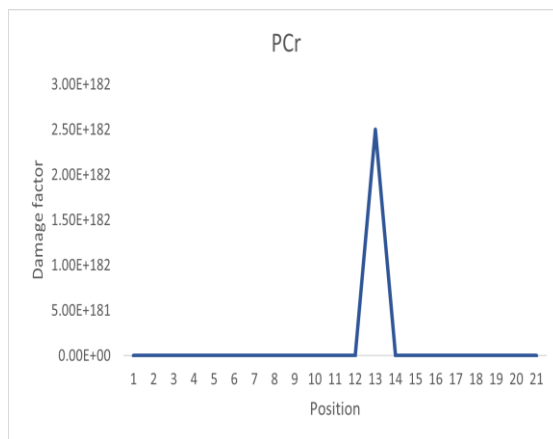


3.Results Validation:

Then these contact pressure for each element has been transformed to the stresses by following the equations and step explained above to get the value damage factor.

Damage factor for each position evaluated from PCr Criterion:

Position	Number of cycles	Damage factor
1	8.13E+04	1.23E-05
2	6.43E+04	1.56E-05
3	4.60E+04	2.17E-05
4	3.32E+04	3.01E-05
5	1.53E+04	6.52E-05
6	9.55E+03	1.05E-04
7	4.53E+03	2.21E-04
8	1.55E+03	6.46E-04
9	2.06E+02	4.87E-03
10	3.02E+01	3.31E-02
11	7.48E+00	1.34E-01
12	1.20E-04	8.35E+03
13	4.00E-183	2.50E+182
14	2.52E-42	3.97E+41
15	1.49E+05	6.70E-06
16	5.93E+04	1.69E-05
17	6.68E+04	1.50E-05
18	6.86E+04	1.46E-05
19	7.81E+04	1.28E-05
20	7.74E+04	1.29E-05
21	9.09E+04	1.10E-05

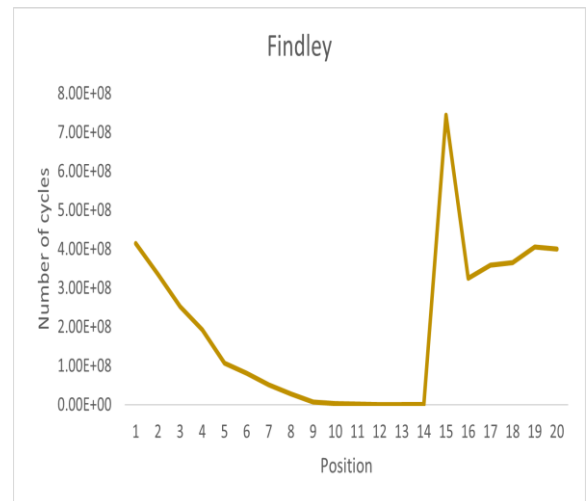
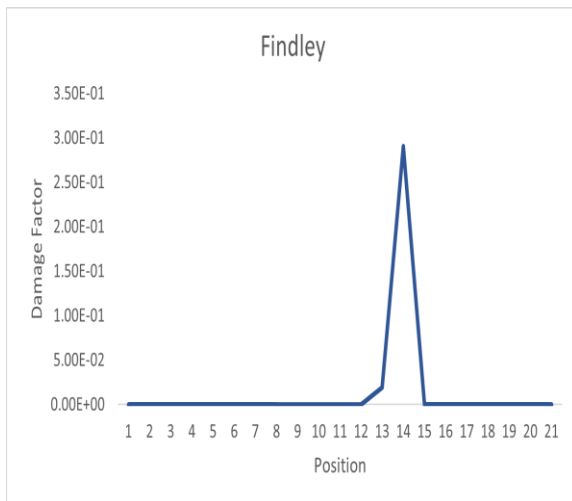


This confirms that PCr criterion cannot provide reasonable values of damage factor or number of cycles to failure at higher values of contact pressures, this can be cross checked from the values of damage factor at position 12, 13, and 14.

3.Results Validation:

Damage factor values for each position evaluated from Findley Criterion:

Position	Number of cycles	Damage factor
1	4.14E+08	2.41E-09
2	3.36E+08	2.98E-09
3	2.52E+08	3.97E-09
4	1.92E+08	5.21E-09
5	1.06E+08	9.40E-09
6	8.08E+07	1.24E-08
7	5.14E+07	1.94E-08
8	2.72E+07	3.68E-08
9	7.40E+06	1.35E-07
10	2.65E+06	3.77E-07
11	1.38E+06	7.25E-07
12	5.08E+04	1.97E-05
13	5.16E+01	1.94E-02
14	3.44E+00	2.91E-01
15	7.44E+08	1.34E-09
16	3.25E+08	3.07E-09
17	3.58E+08	2.79E-09
18	3.65E+08	2.74E-09
19	4.06E+08	2.46E-09
20	4.00E+08	2.50E-09
21	4.60E+08	2.18E-09



Whereas, from Findley criterion the values of damage factor and number of cycles to failure at higher contact pressures are reasonable respect to PCr criterion.

3.3 Case 2- By using realistic values of contact pressures:

In this case the dimension of gears, are of gears we normally have in gearbox. So, the contact pressure values are reasonable. Contact pressure has been evaluated for each element of the mesh of the contact area of the teeth.

In this case total positions considered are 20 positions. Position here is referenced to the number of contacts among the pair of teeth.

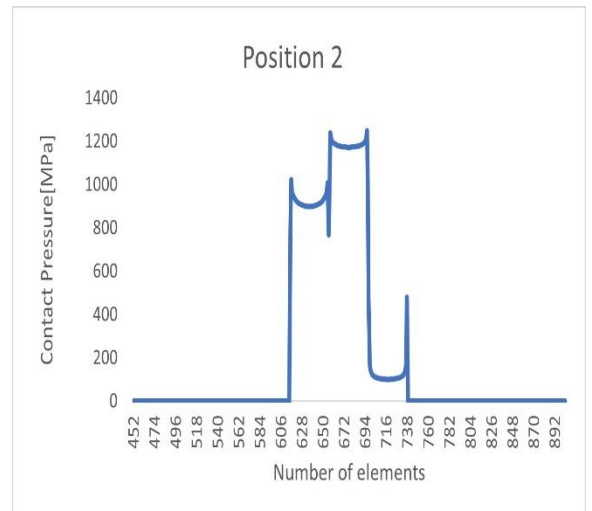
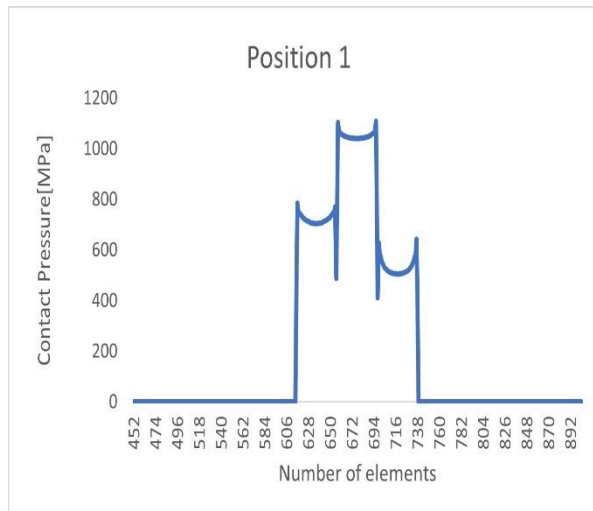
By following FEM analysis and approach mentioned in first Matlab script, contact pressures values has been computed for all pairs of teeth in contact, but for analysis only a pair of teeth considered from 452 to 902 number of elements along the whole pitch line.

Gear pair parameters:

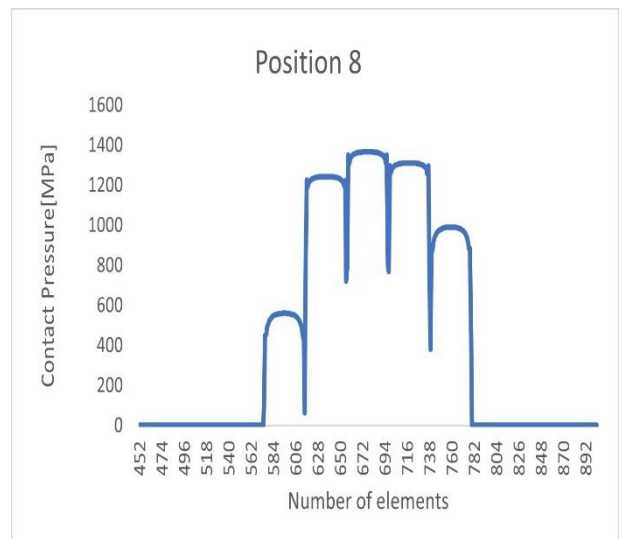
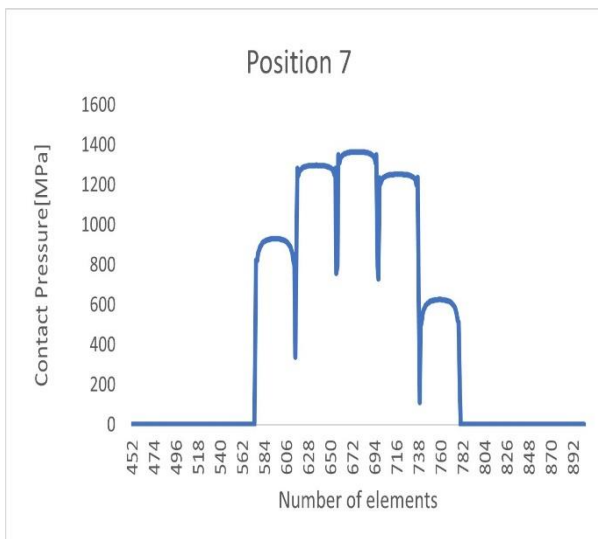
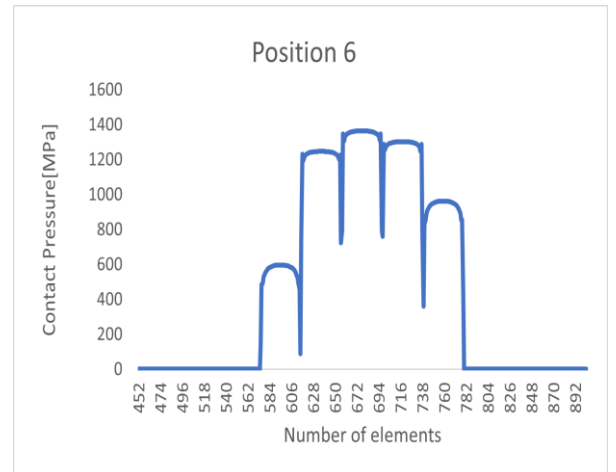
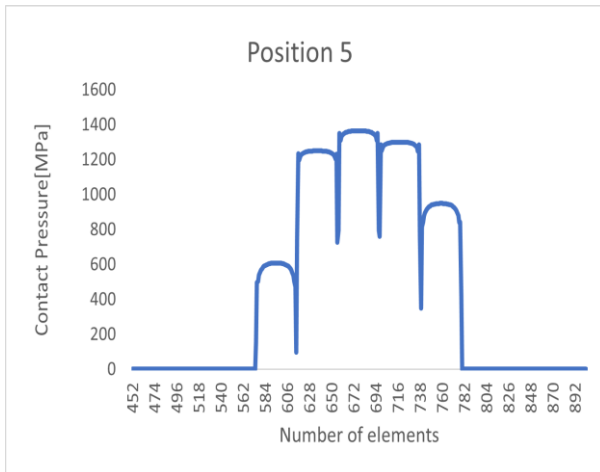
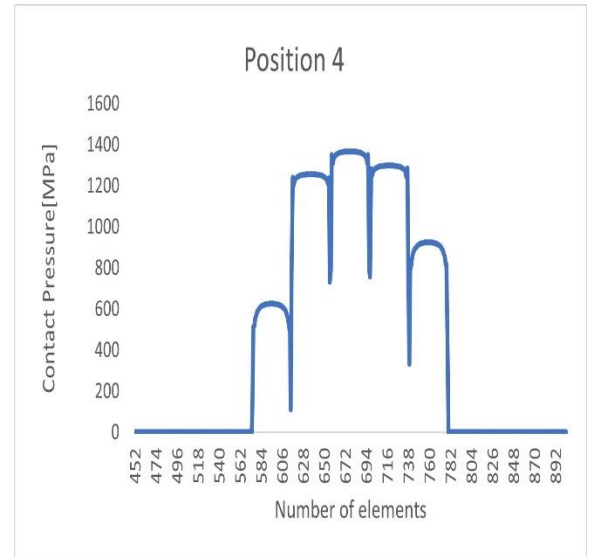
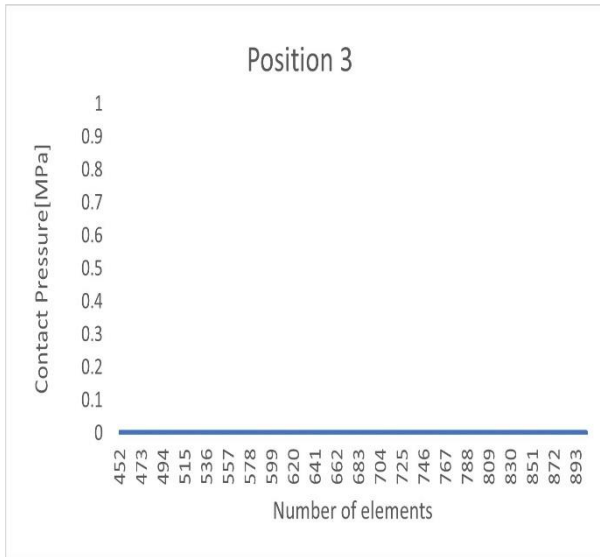
Table 1 Gear pair parameters

Parameter	Pinion p	Gear g
Number of teeth z [-]	28	28
Module m [mm]	3.175	3.175
Pressure angle α_p [°]	20	20
Facewidth b [mm]	6.35	6.35
Hub radius [mm]	20	20
Torque T [Nmm]	101686	
Young modulus E [MPa]	210000	210000
Poisson coefficient ν [-]	0.3	0.3

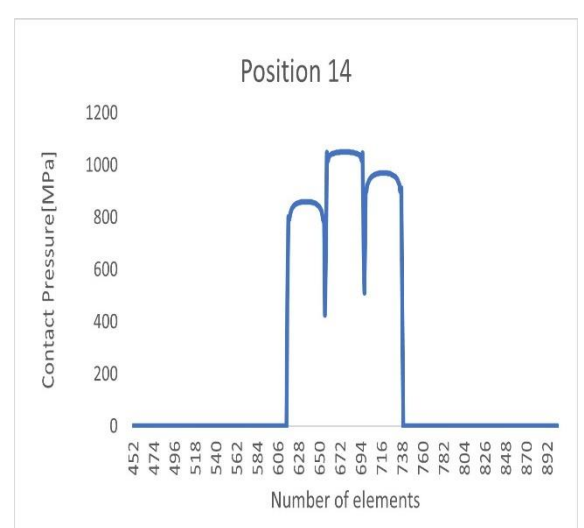
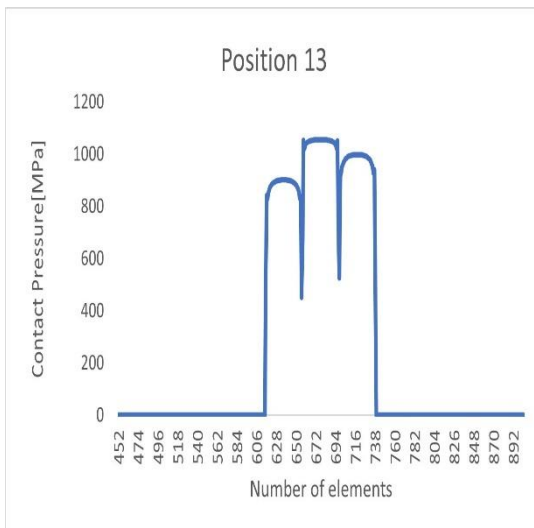
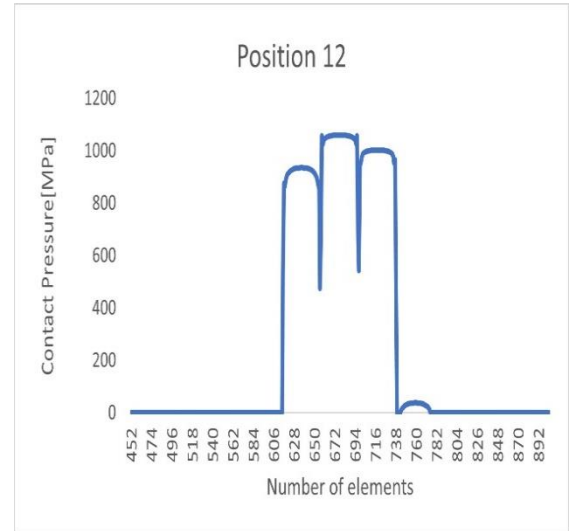
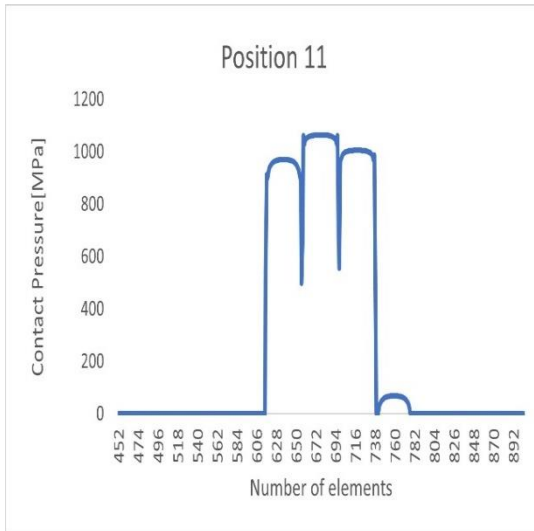
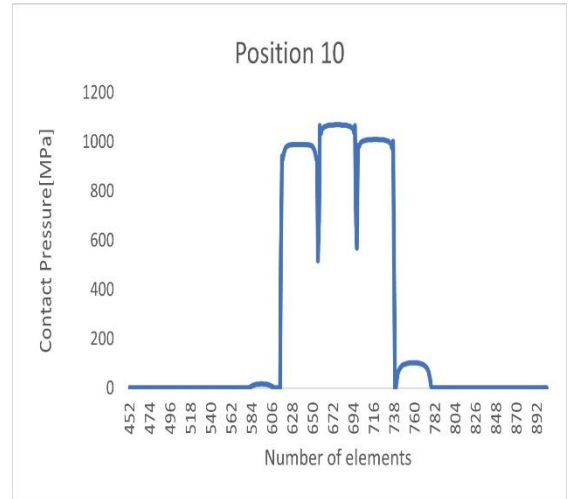
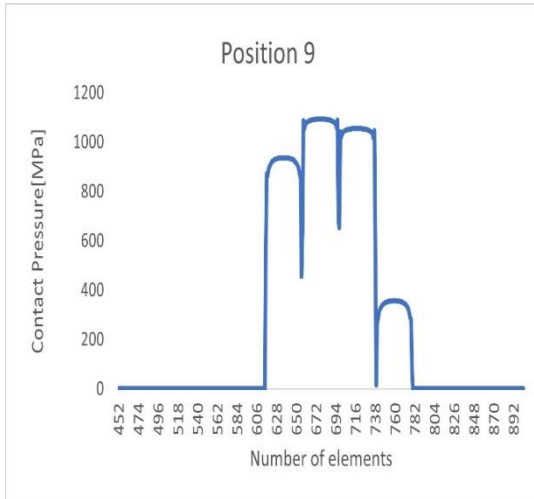
Pressure distribution for each position:



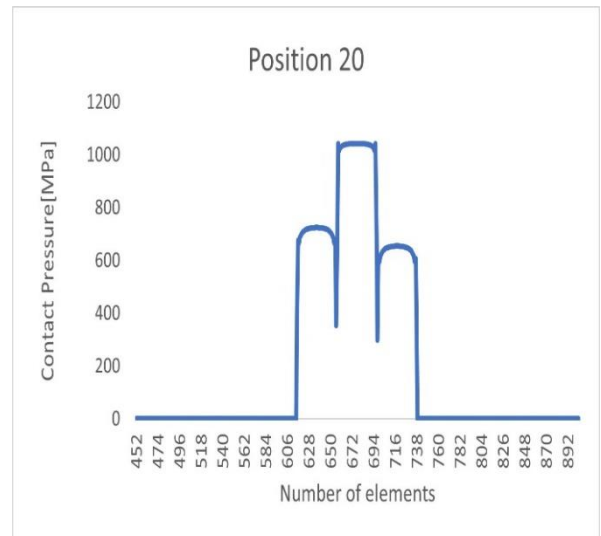
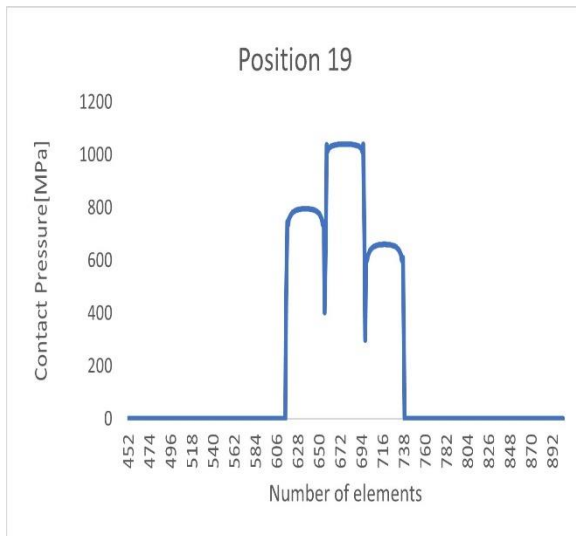
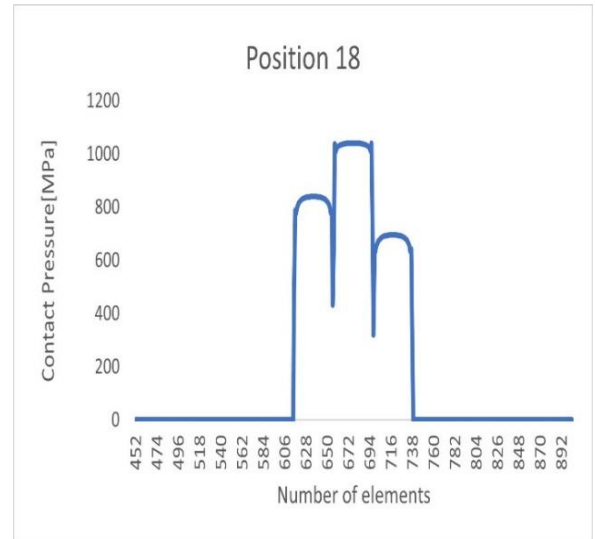
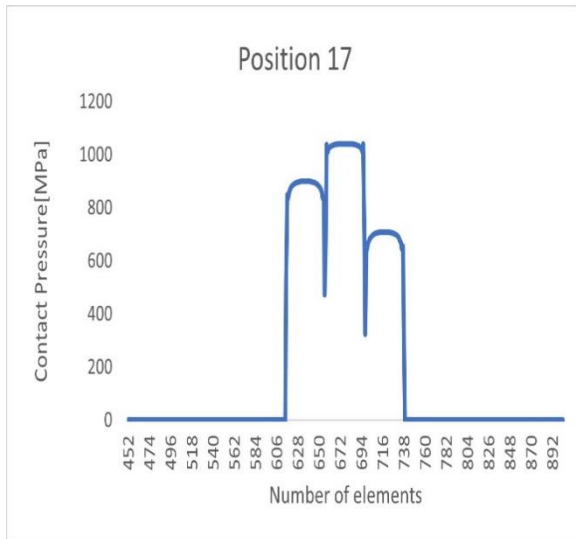
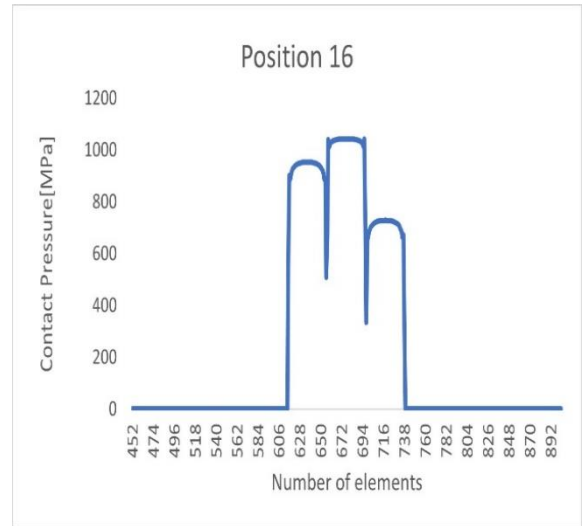
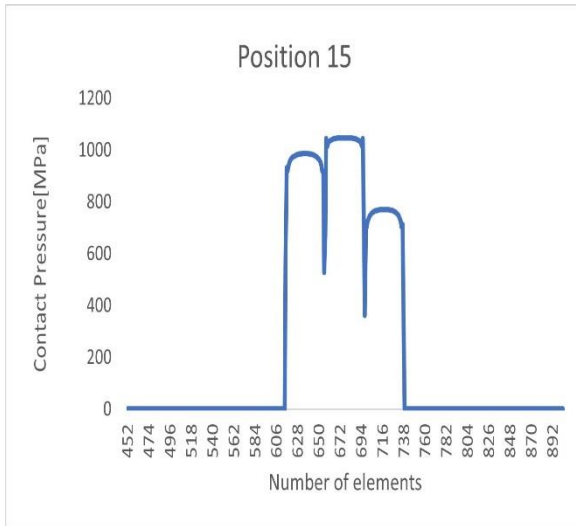
3.Results Validation:



3.Results Validation:



3.Results Validation:



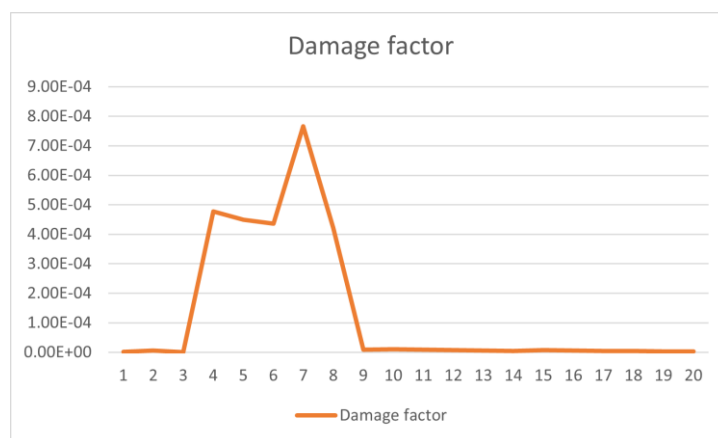
Note: For position 3 the contact pressure is zero because the pair of teeth is not in contact at that position.

3.Results Validation:

Damage factor for each position evaluated from PCr Criterion:

Position	Number of cycles	Damage factor
1	5.75E+05	1.74E-06
2	1.70E+05	5.89E-06
3	Infinity	0.00E+00
4	2.09E+03	4.78E-04
5	2.22E+03	4.50E-04
6	2.29E+03	4.36E-04
7	1.31E+03	7.66E-04
8	2.37E+03	4.21E-04
9	1.08E+05	9.29E-06
10	9.82E+04	1.02E-05
11	1.13E+05	8.89E-06
12	1.37E+05	7.30E-06
13	1.64E+05	6.10E-06
14	2.07E+05	4.83E-06
15	1.32E+05	7.58E-06
16	1.61E+05	6.23E-06
17	2.10E+05	4.76E-06
18	2.81E+05	3.56E-06
19	3.50E+05	2.85E-06
20	4.80E+05	2.08E-06

The values of damage factor are reasonable but still severe compared to Findley Criterion.

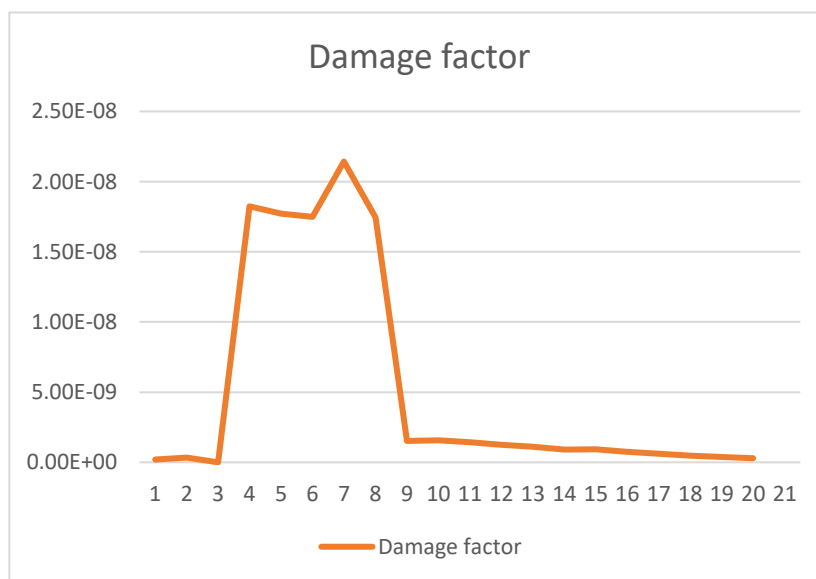


3.Results Validation:

Damage factor for each position evaluated from Findley Criterion:

Position	Number of cycles	Damage factor
1	5.11E+09	1.96E-10
2	2.87E+09	3.48E-10
3	Infinity	0.00E+00
4	5.48E+07	1.82E-08
5	5.64E+07	1.77E-08
6	5.72E+07	1.75E-08
7	4.67E+07	2.14E-08
8	5.73E+07	1.74E-08
9	6.53E+08	1.53E-09
10	6.34E+08	1.58E-09
11	6.95E+08	1.44E-09
12	7.96E+08	1.26E-09
13	9.02E+08	1.11E-09
14	1.12E+09	8.96E-10
15	1.08E+09	9.29E-10
16	1.32E+09	7.56E-10
17	1.66E+09	6.01E-10
18	2.11E+09	4.74E-10
19	2.64E+09	3.79E-10
20	3.41E+09	2.93E-10

Among all the cases the best and most reasonable values of damage factor has been provided by Findley Criterion.



Conclusion

The thesis work starts with the aim to find what are the most common and catastrophic damages that can be found in the gearbox which is under working conditions. And then look for the methodologies to detect these damages in an early stage to avoid the failure of the whole gearbox.

After this step, the objective is finalized to find the correlation between oil debris amount and failure mechanism.

First model gives us the correlation between oil debris amount and wear. The sensitivity analysis of this model has been performed also in order to investigate how the output of the mathematical model changes by changing the input parameters.

Second model gives us the correlation between oil debris amount and pitting. To develop this model the approach is different because the relationship is not direct as the model of wear. Here, the correlation is between number of cycles to failure and the contact stress.

So, with the help of the second model it is also possible to tell that the debris amount caused is by pitting or wear because when the damage factor is equal to one, the possibility to have debris is reached. If debris comes earlier than the number of cycles which corresponds to a damage factor value greater than one, the debris is surely caused by the wear, if not, it is caused by the pitting. Another pro of this model is that it can help to avoid catastrophic failure, because wear happens at the starting phase of the contact, whereas pitting happens at the progressive stage which is more dangerous. So once the debris amount is found and the damage factor value is less than one, we can do countermeasures to reduce wear and can avoid the pitting damage at early stage.

Bibliography

- [1]. S.K. Bhaumik, M. Sujata, M. Suresh Kumar, M.A.Venkataswamy, M.A. Parameswara, “Failure of an intermediate gearbox of a helicopter”.
- [2]. Wei Caoa,c., Han Zhanga , Ning Wanga , Hai Wen Wangb , Zhong Xiao Pengc, “To find a correlation between oil debris amount, caused by two phenomena wear and pitting and failure mechanism”
- [3]. Steffen D. Nyman, Education Coordinator, C.C. JENSEN A/S, “Description of Wear”.
- [4]. Rexnord Industries, LLC, Gear Group, “Failure Analysis Gears-Shafts-Bearings-Seals”.
- [5]. Paula J. Dempsey, Abdollah A. Afjeh, “Integrating Oil Debris and Vibration Gear Damage Detection Technologies Using Fuzzy Logic”.
- [6]. Boualem Merainani, Djamel Benazzouz and Chemseddine Rahmoune, “Early detection of tooth crack damage in gearbox using empirical wavelet transform combined by Hilbert transform”.
- [7]. Amit Aherwar, Md. Saifullah Khalid, “Vibration Analysis Techniques for Gearbox Diagnostic”.
- [8]. J. Torben, Mohamed Ali Fourati, Florian Pape, and Gerhard Poll, “Energy-Based Modelling of Adhesive Wear in the Mixed Lubrication Regime”.
- [9]. Jan Papuga, “A Survey on evaluating the fatigue limit under multiaxial loading”.
- [10]. V. Papadopoulos, “Critical Plane Approaches in High-Cycle Fatigue: On the definition of the amplitude and mean value of the shear stress acting on the critical plane”.
- [11]. Francesco Marmo, Ferdinando Toraldo, Alessandro Rosati, “Numerical solution of smooth and rough contact problems”.
- [12]. J. Reine und Angewandte Mathematik 92, 156–171, “Hertz H (1882) On the contact of elastic solids”.
- [13]. Francesco Marmo, Luciano Rosati, “A general approach to the solution of Boussinesq’s problem for polynomial pressures acting over polygonal domains”.